

LAFAYETTE

SENIOR HONORS THESIS

DEPARTMENT OF MECHANICAL ENGINEERING

Interaction of Cavity Frequencies in Supersonic Combustible Flow

Author:

D. Mac JONES

Advisor:

Dr. Tobias ROSSMANN

Thesis Committee:

Dr. Tobias Rossmann, Chair

Mechanical Engineering

Dr. Daniel Sabatino

Mechanical Engineering

Dr. James Schaefer

Chemical and Biomolecular Engineering

*A thesis submitted in fulfillment of the requirements
for Honors in Mechanical Engineering
in the*



July 2016

Declaration of Authorship

I, D. Mac JONES, declare that this thesis titled, 'Interaction of Cavity Frequencies in Supersonic Combustible Flow' and the work presented in it are my own. I confirm that:

- This work was done wholly or mainly while in candidature for honors in Mechanical Engineering at Lafayette College.
- Where I have consulted the published work of others, this is always clearly attributed.
- Where I have quoted from the work of others, the source is always given. With the exception of such quotations, this thesis is entirely my own work.
- I have acknowledged all main sources of help.
- Where the thesis is based on work done by myself jointly with others, I have made clear exactly what was done by others and what I have contributed myself.

Signed:

Date:

“60% of the time, it works every time.”

Brian Fantana

Abstract

Interaction of Cavity Frequencies in Supersonic Combustible Flow

by D. Mac JONES

LAFAYETTE COLLEGE

Honors in Mechanical Engineering

Mixing and combustion are important aspects of high speed, air breathing engines. These engines, similar to commercial jet engines, use the atmospheric air as the oxidizer in combustion reactions. However, as the speed of the aircraft increases, the time which the fuel and air can mix into the proper proportions for combustion decreases. For flight speeds of Mach 7 and higher, this time could be well under 1ms. The need for enhanced mixing techniques that allow the fuel and air to mix into the proper conditions in these engines has sparked much research. One proposed method to enhance mixing is a rectangular cavity downstream of the fuel injectors. This cavity has been shown to be a promising means for mixing and flame-holding.

Also present in these cavities are strong acoustic waves. As the fuel and air travel over these cavities, pressure waves propagate from the back wall to the front wall. Because of the closed nature of these cavities, these acoustic waves oscillate. These acoustic waves could have the potential to enhance mixing within these cavities further, which could aid in the combustion process as conditions within the engine become less ideal. If the fuel and air proportions are not correct, the combustion in the engine could stop, resulting in a stalled engine. However, with the enhanced mixing of the cavity acoustics, the engine could re-initiate combustion, saving the engine and aircraft.

Utilizing the newly installed expansion tube facility, tests were run with cavity models at engine conditions similar to the conditions that would be experienced by these supersonic, air breathing engines. This investigation will attempt to understand the mechanics of these acoustic waves as they affect mixing and combustion at non-ideal conditions.

Acknowledgements

There are a few people who I would like to acknowledge. First, I would like to acknowledge my research partner, Ray Sanzi. Thank you, Ray, for helping me learn about various compressible flow topics as well as assist me in running tests. I also want to thank you for all the work you put in for our group presentations. We make a pretty good tag team, if I do say so myself. I do not think I could have done this without you.

I would also like to thank my research advisor, Professor Rossmann. With your constant support and overall excitement about this project, I was inspired to complete this thesis. I appreciate all the times you forced me do the various presentations throughout the year. I understand now that you were doing it to make me more comfortable giving presentations, and not to torture me.

And to the rest of the LAUNCH team, I wish you good luck in your own projects. Know that I am always an email away if you need any clarification or advice. I hope this thesis is sufficient for anyone wishing to continue this research project in the future.

Cheers,

Mac

Contents

Declaration of Authorship	i
Abstract	iii
Acknowledgements	iv
Contents	v
List of Figures	vii
List of Tables	viii
Abbreviations	ix
Physical Constants	x
Symbols	xi
1 Introduction	1
1.1 Motivation	1
1.2 Background	4
1.2.1 Acoustic Properties	4
1.2.2 Flame Holding	6
1.2.3 Initiation and Extinction	8
2 Experimental Setup	13
2.1 Expansion Tube	13
2.1.1 Sections	13
2.1.2 Diaphragms	15
2.2 Models	17
2.2.1 Design Choices	18
2.2.2 Modular Design	20
2.2.3 Implementation	21
2.3 High Speed Pressure Transducers	22
2.3.1 Circuit	23
2.4 Infrared Sensor	23
2.4.1 Design of System	24
2.4.2 Absorption	25
2.4.3 Emission	26

2.4.4	Premature Ignition	27
2.5	Schlieren Imaging	27
3	Experimental Results	38
3.1	Non-Combusting Tests	38
3.1.1	Schlieren	38
3.1.2	IR	39
4	Future Work	48
4.1	Future Testing	48
4.2	Suggestions for Other Improvements	49
4.2.1	Fuel Injection into Cavities	50
A	Implementation and Troubleshooting of the Timer Counter Circuit	51
B	Implementation of the IR Sensor	54
C	IR Test Information	56
	Bibliography	57

List of Figures

1.1	Scramjet Diagram	9
1.2	Diagram of typical cavity	9
1.3	Cavity-Actuated Mixing	10
1.4	Diagram of typical cavity showing recirculation	10
1.5	Eddies within a closed cavity	11
1.6	Eddies within an open cavity	11
1.7	Shedding vortex process that occurs within cavities	12
2.1	Annotated Expansion Tube	30
2.2	Cavity Drawing	31
2.3	Cavity in Test Section	32
2.4	Cavity Model with Inserts	32
2.5	Circuit Diagram for Timer Counter Box	33
2.6	Data Flow for High Speed Pressure Transducers	34
2.7	IR setup diagram	35
2.8	Labeled photograph of IR setup	35
2.9	Typical IR data utilizing absorption method	36
2.10	Typical IR data utilizing emission method	36
2.11	Schlieren Diagram	37
3.1	Schlieren image of cavity. L/D = 5.	41
3.2	Schlieren image of cavity with angled downstream wall. L/D = 5.	41
3.3	Schlieren image of cavity. L/D = 7.	42
3.4	Schlieren image of cavity. L/D = 9.	42
3.5	Time-correlated Schlieren image of cavity. L/D = 5.	43
3.6	X-T Diagram of Cavity Tests	44
3.7	IR Signal for Test 046	45
3.8	IR Signal for Test 046	46
3.9	IR Signal for Test 046	47

List of Tables

2.1	Diaphragm Burst Pressures	16
3.1	Test time calculated with IR signal	40
A.1	Digital Pin Out Colors	53
C.1	Basic pressure, timer counter, IR, and test time data from all successful tests utilizing the IR sensor. The test gas labeled CO ₂ was a 5% CO ₂ mixture in nitrogen. The test gas labeled H ₂ was a 2H ₂ + O ₂ + 8N ₂ mixture. *Staged filling resulted in two levels of IR signal. The first number represents the time the Hydrogen mixture passed the sensor, while the second represents the CO ₂ mixture.	56

Abbreviations

FPS Frames Per Second

L/D Length to Depth

TTL Transistor Transistor Logic

Physical Constants

Empirical Constant $\alpha = 0.25$ (for cavities with L/D > 4)

Empirical Constant $k = 0.57$ (for cavities with L/D > 4)

Symbols

m	mode number	
M_∞	Freestream Mach Number	
Re_x	Reynolds number	
U_∞	Freestream Velocity	m/s
γ_∞	Freestream Specific Heat Ratio	
ρ	Density of test gas	kg/m^3
μ	Viscosity of test gas	$kg/m \cdot s$

Chapter 1

Introduction

1.1 Motivation

Supersonic combusting ramjet, or scramjet, engines are on the forefront of supersonic transportation development because of their simplicity and promising outlook for steady and reliable supersonic combustion. These engines differ from typical subsonic jet engines, as scramjets have no moving parts and simply rely on shock waves produced at these supersonic speeds to compress the intake air and provide the means for ignition.

Shown in Figure 1.1 is a diagram of a typical scramjet engine.

One challenge facing the production of these engines is producing steady combustion. Much like keeping a match lit in a hurricane, keeping a flame stabilized at supersonic speeds is quite difficult. One proposed method of flame stabilization is a rectangular cavity, as shown in Figure 1.2. These cavities, are able provide a re-circulation zone with high temperatures and combustion radicals for strong combustion to occur. Many experimental studies have tested the flame-holding abilities of cavities in strong combustion cases [1–4]. Strong combustion occurs when the fuel-air mixture is optimized for

efficient fuel burning. The mixture in strong combustion cases occur in proper stoichiometric proportions. These studies focused on cavity dimensions and how the length to depth ratio, L/D, affects key ignition and flame holding characteristics, such as stagnation pressure, stagnation temperature, fuel air mixture, and residence time. Ben-Yakar concluded that with L/D ratios between 4 and 10, strong combustion can be sustained in these cavities for total enthalpy flight conditions of Mach 8, 10, and 13[2]. Also noted in several investigations is the presence of strong acoustic waves[5–10].

Similar to blowing air over an empty bottle to create a tone, the freestream air traveling over and interacting with these cavities produces acoustic waves. In these cavities, a shear layer develops between the high speed freestream and the slower, re-circulating air in the cavity. As the shear layer travels downstream, it begins to drop. This drop in the shear layer is caused by a pressure gradient present between the freestream and the cavity. When the cavity is long ($L/D > 20$), there is only a small eddy in the upstream corner of the cavity. The eddy created is not strong enough to keep the shear layer out of the cavity, and thus the shear layer grows into the cavity. In these long cavities, the shear layer can grow to the bottom of the cavity, entraining mass from the cavity. In smaller cavities ($L/D \sim 5$), the eddy is relatively larger, taking up nearly the entire cavity. This strong eddy inhibits the mass transfer from the cavity to the shear layer, making the shear layer smaller and less likely to grow into the cavity. Also, in these smaller cavities, there is a stronger pressure gradient, making it harder for the shear layer to grow into the cavity. However, due to the unsteady nature of the flow and the pressure gradient, the shear layer can still dip into the cavity. By the time the shear layer reaches the downstream wall of the cavity, it has lowered to a point where the interaction of the shear layer with the downstream wall of the cavity produces strong pressure waves, which propagate upstream, ultimately resonating within the cavity.

Other experimental studies have investigated the acoustic properties of these cavities [5–10]. These investigations concluded that the acoustic waves generated by supersonic cavities produce several undesirable effects. One effect, investigated by McGregor is the induced drag associated with rectangular cavities. The effect of pressure waves within these cavities can increase the drag by as much as 250% [8]. These acoustic waves can also have an adverse effect on equipment and the crew. At low frequencies, the resonating acoustic waves can cause structural damage to the engine. At high frequencies, these waves can cause uneasiness in crew members [8].

Conclusions drawn from these investigations have led to the desire to suppress these acoustic waves. Suppressing these waves would reduce drag on the engine and cause less damage to the engine or the crew. However, stabilizing these acoustic waves could reduce the effectiveness of these cavities because mass transfer and residence time are important to flame holding [2]. These acoustic waves could also have the potential to assist in combustion when conditions for weak combustion are present. Weak combustion, as is studied in this investigation, is at lean fuel air mixture conditions. Sato et al.[10] investigated the enhancement of mixing due to acoustic waves. They concluded that mixing was enhanced by these acoustic waves and the rate of enhancement was controlled by the cavity’s shape. However, the investigations performed by Sato et al. did not include the cavity as a flame-holder. The cavity was only used to produce the mixing enhancing acoustic waves.

One study, though, focused on the ability of cavity-induced acoustic waves to enhance mixing [10]. Their experimental setup, as shown in Figure 1.3 shows that the wall-mounted cavities were used exclusively as acoustic wave generators to enhance the mixing of the freestream and the injected gas. Their study showed that the cavity acoustic waves produced had enough energy to enhance mixing. This study will attempt to combine

the flame-holding characteristics of these cavities with the acoustic wave assisted mixing. One main difference between Sato's study and this investigation is the location of the enhanced mixing. In this study, the primary focus of studying the acoustic waves is to understand their mixing properties within the flame-holding cavities, rather than outside the cavity. The acoustic waves generated inside the cavity should have nearly the same strength as the waves that escaped the cavity in Sato's study. Because of this, the mixing effects observed in Sato's study should also be present and observable within these flame-holding cavities.

Few, if any, experimental studies have investigated the acoustic properties of these cavities as they assist in mixing and the enhancement of combustion at lean conditions. This investigation is broken into three parts: acoustic properties of cavities, flame-holding properties of cavities, and initiation and extinction. Together, these provide a clear interpretation of a cavity's suitability as an effective flame holder during weak combustion conditions. It is the goal of the investigation to show that the acoustic waves present in these cavities play a significant role in mixing, providing enhanced mixing in lean conditions to stabilize the reaction until more stable engine conditions are achieved.

1.2 Background

1.2.1 Acoustic Properties

The first part of the investigation isolated the acoustic properties of the cavities. To calculate the frequency inside the cavity, a modification derived from Rossiter's semi-empirical formula, shown in Equation 1.1, was used. This relationship is able to incorporate the coupling that exists between the acoustic waves and the vortex shedding[11].

However, this relationship does not take into consideration the compressibility effects within the cavity. For this investigation, the frequency of a cavity was estimated using an empirical equation derived by Heller and Delfs [6], as shown in Equation 1.2. Heller and Delfs modified the equation based on their investigation to account for compressibility effects and higher speed of sound within the cavity [2]. The Heller and Delfs equation is estimated to be able to predict the frequency within the cavity $\pm 10\%$ [6].

$$f_m = \frac{m - \alpha}{\{M_\infty + 1/k\}} \cdot \frac{U_\infty}{L} \quad (1.1)$$

$$f_m = \frac{m - \alpha}{\{M_\infty / \sqrt{1 + [(\gamma_\infty - 1)/2]M_\infty^2} + 1/k\}} \cdot \frac{U_\infty}{L} \quad (1.2)$$

Depending on the mode of the strongest acoustic waves, frequencies of these waves will be expected to be between 16.7kHz and 30 kHz for the first mode. It was observed that as L/D increases, the dominant oscillatory mode also increases [2]. However, these base modes should be present within the cavities modeled, but they may not be the strongest modes. For this part of the investigation, three L/D ratios will be investigated: 5, 7, and 9. From the equation, it can be seen that the frequency generated by the cavity is a function of the freestream test gas conditions and length of the cavity. Keeping the freestream conditions nearly identical while changing the length of the cavity will produce different frequencies within the cavity. Data from these tests will lead to the direct comparison of the acoustic properties of the cavities, such as frequency and relative strength, as a function of cavity frequency. Also investigated at each of the L/D ratios was an angled downstream wall to observe the passive suppression of the normally present acoustic waves, as illustrated in Figure 1.4

1.2.2 Flame Holding

The second part of the investigation will be used to isolate the combustion and flame-holding properties of the cavities. As shown by the investigations of Ben-Yakar, L/D ratios between 4 and 10 can sustain strong combustion in these cavities [2]. Because this is a new experiment with a new expansion tube facility, it is important to confirm the flame-holding capabilities of these cavities for the environments that can be achieved. For testing, a strong, stoichiometric, fuel-air mixture will be used and each L/D ratio will be tested, along with its angled downstream wall counterpart. If the cavity model shows promising results of flame-holding, the fuel-air mixture will then be diluted with nitrogen to observe the effects of the acoustic waves as the combustion becomes weaker, which is the third part of this investigation.

For flame holding to occur, certain conditions must be met within the cavity. One of these conditions is recirculation, as illustrated in Figure 1.4. Recirculation within the cavity allows the fuel and air to slow down and mix to the proper stoichiometric conditions before igniting. The physical parameters of the cavity affect this recirculation. For cavities with a L/D ratio of greater than 10-13 are considered closed cavities, as shown in Figure 1.5. Closed cavities do not provide sufficient mass transfer between the freestream and the cavity for proper recirculation. The length of the cavity allows for the shear layer to drop within the cavity due to a pressure gradient between the cavity and the freestream, effectively creating two weak eddies within the cavity. These eddies are not strong enough to escape into the freestream. However, cavities with a L/D ratio between 4 and 10 do not experience this significant drop in the shear layer, resulting in one strong eddy within the cavity, as illustrated in Figure 1.6. These cavities are considered open, and are strong enough to provide sufficient mass transfer between the cavity

and the freestream, resulting in effective recirculation [1]. Computational investigations by Gruber et al. show that there exists one large vortex near the downstream edge of the cavity and a secondary vortex exists near the upstream wall of an open cavity [12]. This downstream vortex, which interacts with the unstable shear layer, controls the mass transfer between the cavity and the freestream gas. This process is illustrated in Figure 1.7.

The recirculation of a cavity is characterized by its residence time. The residence time is the amount of time in which the test gas remains within the cavity. For the air-breathing scramjet engines, residence time is particularly important. The fuel and air have less than 1ms to mix and ignite, so any extra time the cavity gives to the mixing and ignition process has the potential to be extremely useful. Previous cavity investigations have shown that cavities can provide residence times on the order of 1ms, effectively doubling the amount of time the fuel and air have to mix and ignite.

One last feature of the cavities is that they provide a hot anchor point for the flame. The initial step of the cavity causes a shear layer to form, which separates the high velocity freestream from the low velocity mixing flow within the cavity. When the freestream gas slows down in the cavity, the kinetic energy within the flow is converted into mostly thermal energy. This increases the temperature within the cavity, providing a "hot zone," which is hot enough for auto-ignition of the fuel-air mixture. The hot zone provides a point which the flame can latch onto and stabilize itself to continue the combustion process.

1.2.3 Initiation and Extinction

The third part of the investigation is used to observe the effect that the acoustic waves have on the flame-holding characteristics of the cavities in a non-stoichiometric fuel-air mixture. For these experiments, both flat and angled wall cavities will be tested at the same conditions. Shown by results of the acoustic investigation, the angled walls do suppress the propagating acoustic waves within the cavity, so any observable differences between the results of the angled versus flat downstream wall will be assumed to be due to the cavity acoustics. Ideally, the results of these tests would be to show that the flat downstream wall, and thus the cavity acoustics, do enhance the mixing of the fuel and air, producing stronger combustion than the angled downstream wall. More details about this investigation are included in the Future Works section of this thesis, Chapter 4.

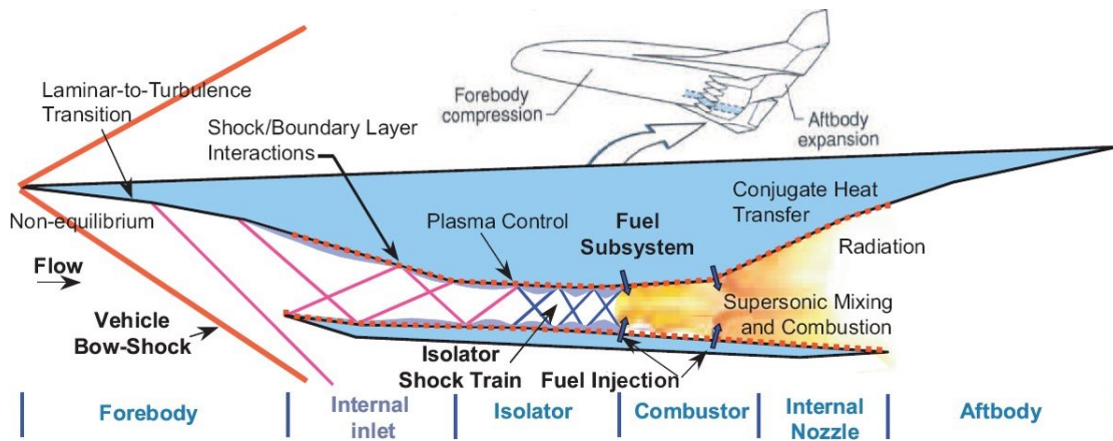


FIGURE 1.1: Diagram of a typical scramjet engine, showing shocks produced within the engine. [13]

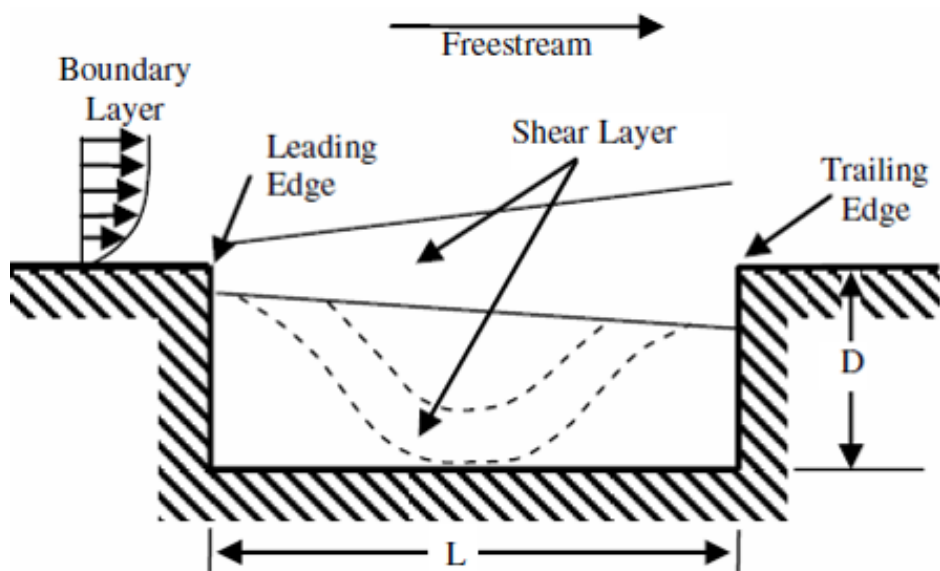


FIGURE 1.2: Typical hypersonic cavity schematic [14].

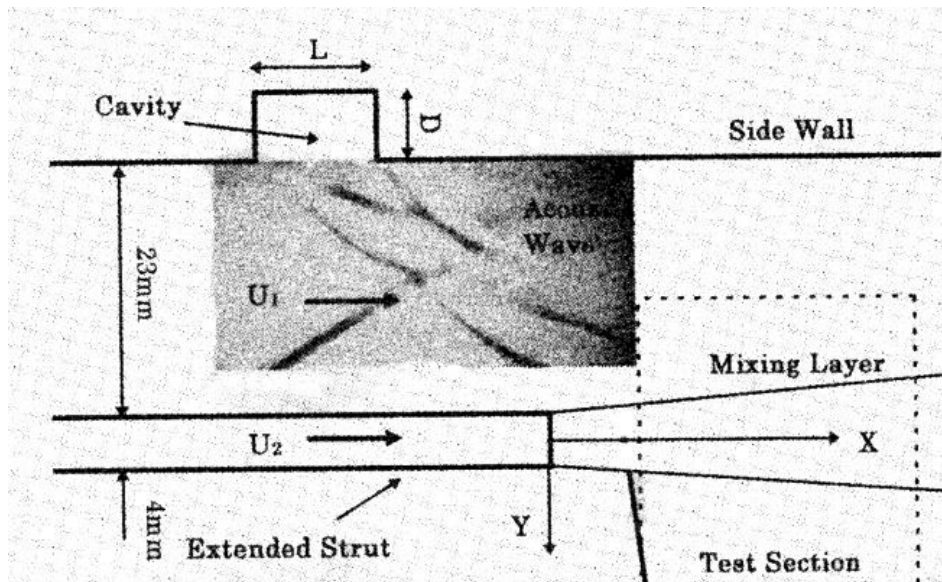


FIGURE 1.3: Mixing enhanced by acoustic waves produced by a side wall-mounted cavity [10]



FIGURE 1.4: Typical hypersonic cavity schematic showing recirculation and angled downstream wall [3].

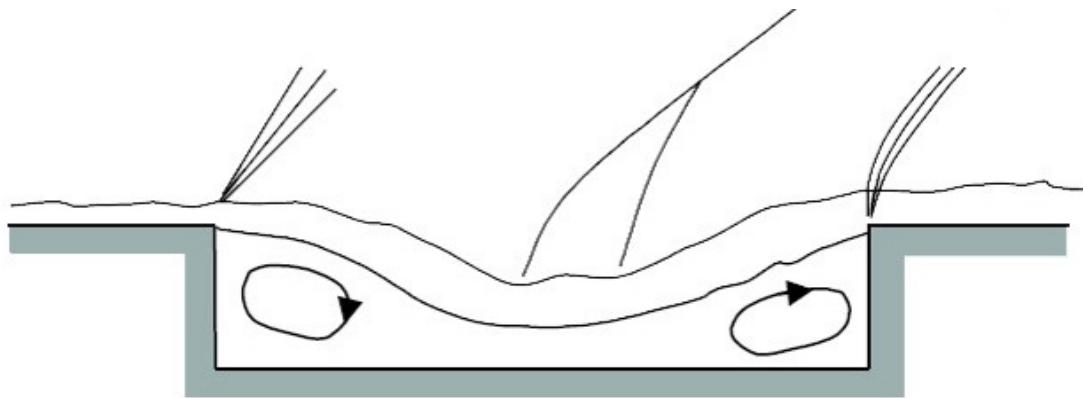


FIGURE 1.5: Eddies within a closed cavity [1]. The shear layer drops into the cavity, creating two separate, weak eddies. The eddies are not strong enough to provide the mass transfer between the cavity and the freestream needed for stable combustion.

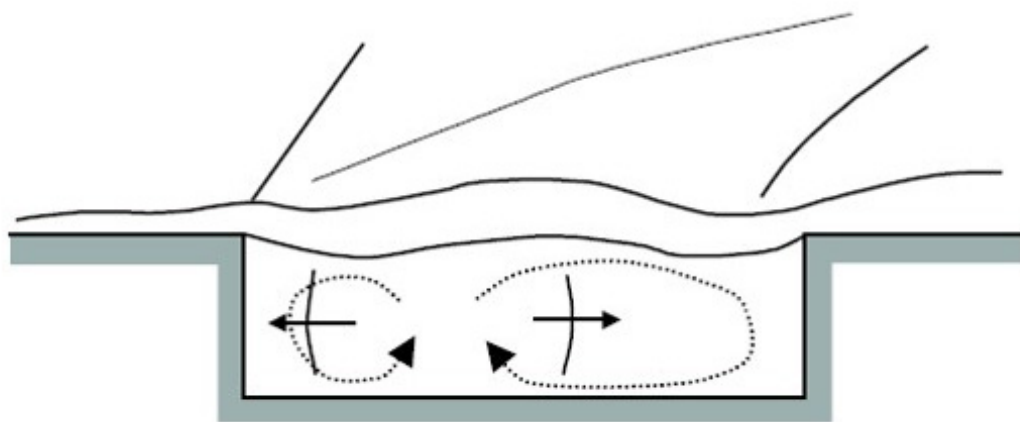


FIGURE 1.6: Eddies within an open cavity [1]. The eddies formed in an open cavity are strong enough to expel mixed fuel and air into the freestream, allowing stable combustion to occur.

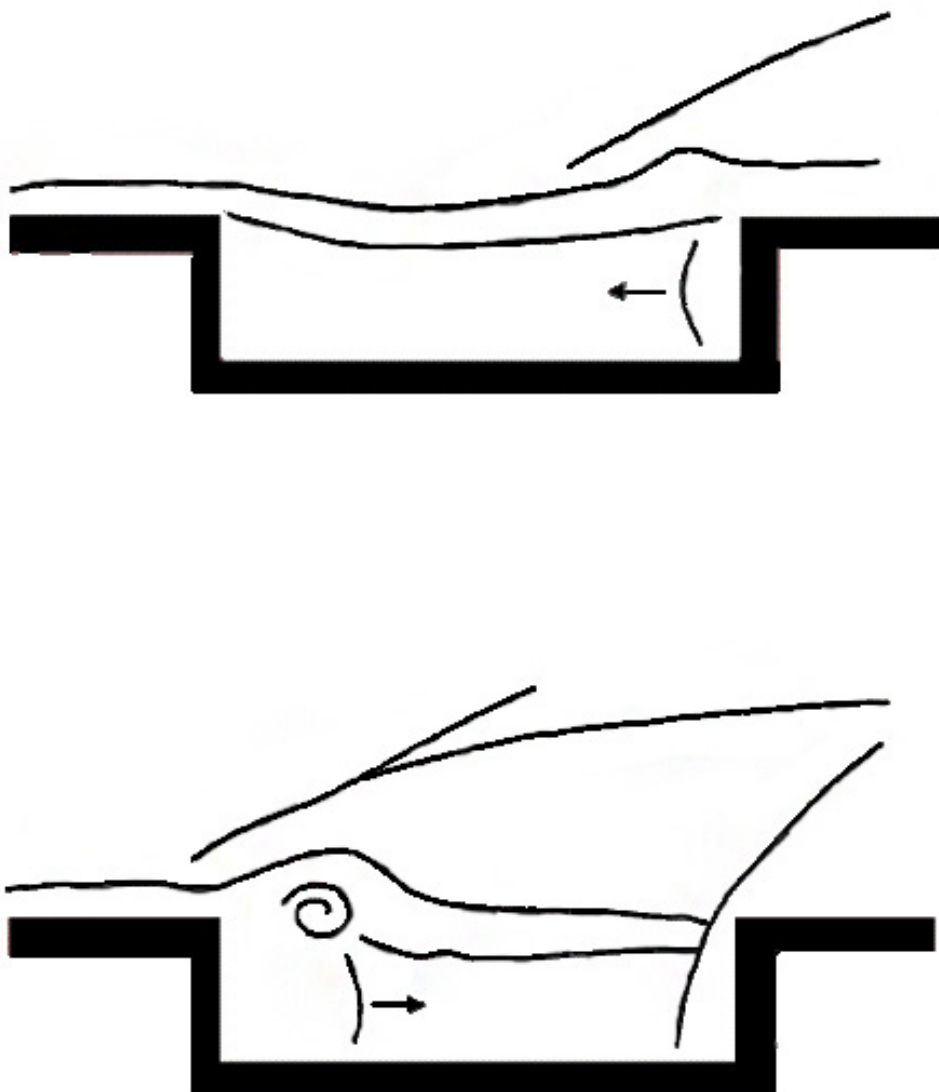


FIGURE 1.7: Shedding vortex process that occurs within cavities [1]. Shear layer first interacts with downstream wall, producing a pressure wave that travels upstream (above). These pressure waves interact with the upstream wall and assist in shedding vortices from the leading edge (below).

Chapter 2

Experimental Setup

2.1 Expansion Tube

In order to achieve the proper flow conditions to mimic conditions experienced in true hypersonic engines, an expansion tube is utilized. The expansion tube is an impulse flow device similar to a shock tube. With an expansion tube, a high pressure gas is used to accelerate a volume of lower pressure gas to certain conditions required for supersonic testing. For the case of supersonic cavities, these conditions need to be similar to those found in the combustor of a scramjet engine. With the expansion tube at Lafayette College, Mach numbers between 2 and 4 have been attained. For more details on the specifics of the expansion tube at Lafayette College, including expansion tube theory and the construction of the facility at Lafayette, refer to Helen Hutchens thesis [15]

2.1.1 Sections

The expansion tube consists of four sections, which are highlighted in Figure 2.1. The four sections are: the driver, the double diaphragm, the driven, and the expansion, as

listed from upstream to downstream. Initial conditions of the tube set by the operator determine test conditions within test section. These initial conditions include pressure ratios between the sections as well as the gases used in the sections. Each section is divided by plastic diaphragms at the start of each tests. These diaphragms allow the sections to be filled to the different pressures with the different gases required for testing.

The driver section is contained at a high pressure at the start of a test. This section is rated to 800 psi. Non-combusting tests performed were run with a driver pressure of 225 psi. With higher pressures, faster test velocities of the test gas can be achieved.

The double diaphragm serves as a starting mechanism for the experiments. It is filled to an intermediate pressure about half the driver pressure. This section is a very small volume (58 in^3), which when vented, rapidly creates a large pressure drop across the most upstream diaphragm, causing it to break. The breaking of the diaphragm begins a chain reaction, starting the test.

Once the test begins, the test gas, which is contained in the driven section at a sub-atmospheric pressure, is accelerated by the driver gas. The test gas travels down the tube, compressed and shock heated until it breaks through the last diaphragm between the driven and expansion sections. This last section differentiates an expansion tube from a shock tube. With the addition of the last diaphragm, the expansion section can be kept at an even lower pressure than the driven section. When the diaphragm between these sections break, the test gas experiences expansion and unsteady acceleration, allowing faster freestream velocities and higher Mach numbers in the test section.

2.1.2 Diaphragms

To separate the four sections, plastic diaphragms were placed at the boundary between these sections. These diaphragms were used to keep a pressure differential between the driver, double diaphragm, and driven sections. The pressure differential between these sections was a maximum of 120 psi for non-combusting tests. Another diaphragm was used to separate the test gas in the driver and the expansion gas in the expansion section. Depending on the test conditions, this diaphragm was required to withstand a maximum pressure differential of 1 psi.

Different thickness diaphragms were required, depending on the pressure differential between the sections. All diaphragms used for the driver and double diaphragm sections were cut from polycarbonate sheet. In order to determine the required diaphragm thickness, calculations were performed, utilizing known material properties and spherical pressure vessel relationships. Since the diaphragm is expected to expand to a near half sphere before breaking, a thin wall spherical pressure vessel relationship was used to determine the maximum pressure the plastic could withstand. This relationship, shown in Equation 2.1, was utilized to determine a range of thicknesses of the polycarbonate sheets to be used for different pressure conditions [16].

$$\sigma_{uts} = \frac{P r}{2t} \quad (2.1)$$

After initial testing of these diaphragms, it was determined this relationship provided an overestimation of about 185% for the breaking pressure of a specific thickness of diaphragm. Since the polycarbonate sheets come in standardized stock thicknesses, several thicknesses were purchased and testing was performed to determine the breaking

Thickness (inches)	Trial 1 Burst Pressure (psi)	Trial 2 Burst Pressure (psi)
0.010	32	n/a
0.015	60	n/a
0.020	93	92
0.030	123	125
0.045	153	163
1/16	233	274
3/32	341	n/a

TABLE 2.1: Diaphragm burst pressures at various thicknesses of polycarbonate sheets.

pressure of each diaphragm. For this testing, a 1/4" polycarbonate sheet was placed at the upstream end of the double diaphragm and the thinner test sample was placed at the downstream end of the double diaphragm. The double diaphragm was then filled slowly. When the downstream diaphragm broke, the highest pressure reached was recorded. This procedure was repeated for other thicknesses of diaphragms. The results from these burst tests is shown in Table 2.1. A majority of the non-combusting tests run were at a driver pressure of 225 psi, so 0.045" diaphragms were selected, as they have a higher burst pressure than the pressure differential between the driven and the double diaphragm, but not higher than the differential between the driver and the driven sections. These diaphragms reliably broke for each test.

Occasionally, after a test was run, it was noticed that the pieces of the diaphragm completely broke off, sending these pieces down the tube. Having these large pieces of diaphragm sent down the tube is unwanted. These large pieces can cause serious damage to the model in the test section, as well as damage to other parts of the tube. During one test, a large piece of diaphragm struck the nose of the blunted cylinder model, causing severe damage to the pressure transducer located at the nose. It was also observed that pieces of diaphragm nicked the observation windows on the test section. This type of damage needed to be avoided, so one proposed solution to this problem was to score the diaphragms. A 5 inch, very shallow incision on both sides of the plastic in an "X"

pattern centered on the diaphragm would create failure modes which the diaphragm should break along. These failure modes cause the diaphragm to petal, ideally opening as wide as the tube, with the entire diaphragm intact.

Burst tests were performed on several scored diaphragms of 0.045" thickness. This scoring was performed by hand with a knife, applying light pressure. The resulting score appeared as deep scratches in an "X" pattern. The results of the tests showed no significant decrease in burst pressure. In fact, all of the tests showed a higher burst pressure for the scored diaphragms than for the not scored ones. This could be due to the scoring allowing the plastic to deform further before bursting. Regardless of the reason, the results showed that the scored diaphragms could still be used. It was also found that good petalling of the diaphragm occurred, with minimal, if any, loss of diaphragm pieces down the tube. Because of these results, scoring of the diaphragms has become a regular step in the setup of the tube for each test.

2.2 Models

For testing, a cavity model was designed and manufactured. The designed cavity, as shown in Figure 2.2, was designed to be mounted with the current mounting system in the test section. This mounting system consists of a rectangular upright with thru holes for shoulder bolts. The three holes seen in Figure 2.2 are in line with the existing holes in the mounting system. This allows one to swap out models in the test section quickly in between tests.

2.2.1 Design Choices

While designing the cavity, several choices had to be made about the geometry of the model as well as the features of the cavity. Brass was chosen as the material due to its relatively low cost as well as its ability to be easily machined. Brass also holds up well to the conditions experienced in the test section during testing.

The overall size of the brass was chosen based on the size of the core flow, the flow volume where the desired freestream conditions exist, exiting the tube into the test section as well as the requirement to be affixed to the existing mounting system. The size of the core flow coming out of the tube begins about the diameter of the tube itself. However, it grows smaller as the length from the tube exit increases. It is important that the area of interest (the cavity) is contained entirely within this core flow. Knowing the cavity would sit a few inches from exit of the tube, a width of 2.5 inches was chosen for the brass. This would ensure that the core flow, at the time it interacts with the cavity, would entirely encapsulate the cavity. A total height of 1 inch was chosen because it allowed the rectangular hole for the mounting system to be machined to the correct depth that aligned the thru holes for the shoulder bolts. It was designed such that after the rectangular hole was made in the brass, a thickness of 0.25 inch was left. This was chosen because the cavity exists relatively close to the mounting system and at least 0.125 inch of material needed to be left between the top of the mounting system and the bottom of the cavity to ensure the part could be machined without any issues.

The cavity itself was placed 3.375 inches from the front in order to develop the flow over the flat plate. Flow conditions experienced by the cavity should match closely to flow conditions experienced in scramjet engines, including boundary layer conditions. The thickness of the boundary layer at the upstream edge was estimated to be on the

order of 2mm for the length chosen. This estimation was made using the relationship shown in Equation 2.2, where Re is shown by the relationship in Equation 2.3 and x is the distance to the front of the cavity from the leading edge of the model [17]. For consistency with other researchers and their boundary layer thickness, a length of 3.375 inches was chosen.

$$\delta = \frac{0.37x}{(Re_x)^{1/5}} \quad (2.2)$$

$$Re_x = \frac{\rho U_\infty x}{\mu} \quad (2.3)$$

At the upstream end of the cavity model, there exists a wedge. Flow over a flat plate leading up to the cavity was desired. The wedge was designed in order to redirect any shock waves away from the cavity. These shock waves have the ability to adversely affect test results if they interact with the cavity. Calculating shock wave angles for several wedge angles and calculating where the shocks would reflect off the walls of the test section, a wedge angle of 20° was chosen. This angle created a shock of about 46° for a freestream mach number M_∞ of 2.5 and a specific heat ratio, γ of 1.4, which are conditions similar to the ones that will be run for the cavities. When reflected through the shear layers surrounding the expansion tube core flow, the oblique shock produced would not reflect into the cavity.

The stability of the model was also an important design consideration. With the flow conditions experienced in the test section, a stagnation pressure of nearly 1,000 psi could be experienced by the model. With the model's front wedge shape, a net force in the vertical direction of nearly 3,300 lbs., coupled with a relatively large moment arm has

the potential to result in some movement from the cavity. Initial calculations of bending resulted in a maximum deflection of approximately 0.05 inches. These calculations assumed the model to have a uniform rectangular cross section and all the force was in the center of the wedge. To ensure the bending was as minimal as possible, a triangular brace was manufactured to secure the base of the cavity to the test model stand. This reduced the effective moment arm to provide structural support and stability to the model. This triangular support is pictured in the test section assembly in Figure 2.3.

2.2.2 Modular Design

Because the acoustic properties are the main focus of this thesis, it was important to design a model in which these acoustic properties could change. Frequency is one main acoustic property that was chosen to be varied with these cavities. Using Heller and Delfs relationship, Equation 1.2, varying the length of the cavity would lead to different cavity frequencies [6]. However, the L/D is also an important parameter in the flame-holding characteristics of these cavities. This ratio determines the recirculation properties as well as residence time within the cavity. A modular design was then chosen so that a range of L/D ratios could be tested. For good flame-holding characteristics, a L/D between 4 and 10 has been shown to provide those characteristics [2]. For the design, having a constant depth would result in a change in length of the cavity with a change in L/D ratio. Thus, as the L/D ratio changes, so do the flame holding properties as well as the dominant frequencies within these cavities.

For the modular design, a 1/8-inch deep, 1 5/8-inch long cavity was created, as shown in Figure 2.2. Along with the large cavity, different sized inserts were manufactured. The length of the cavity was chosen so that these inserts could be attached, decreasing the overall length of the cavity, and achieving the desired L/D. Six inserts were manufactured

to create L/Ds of 5, 7, and 9, each with two variants of a downstream wall. These inserts are shown relative to the base cavity in Figure 2.4. At each L/D, there was one insert with a flat wall and one insert manufactured with a 30° incline. This angled incline, as shown by Ben-Yakar [2], has the ability to suppress the acoustic waves while still retaining flame holding characteristics. The angled wall does not allow the pressure waves to propagate within the cavity space. This allowed for the comparison of flame-holding abilities of the cavity with and without strong acoustic waves present at each L/D. This modular design gave a relatively wide spectrum of cavity conditions to test with a relatively easy means of changing these conditions for each test.

2.2.3 Implementation

For each test, it was determined which L/D needed to be tested. After this choice was made, the corresponding insert was installed and the test section mount was prepared for the cavity model to be placed in it. Depending on which model was mounted in the test section before the cavity test, the mounting stand may have needed to be adjusted upstream or downstream in the test section. Since the area of interest is the cavity, it was placed at the center of the viewing window for the schlieren to focus directly on it. Further information on the schlieren system is presented in Section 2.5. Once the test mount was correctly positioned, the cavity model was attached to it with three shoulder bolts. The triangle support was then attached between the model and test stand, providing extra stability when the test runs. Once the model was mounted, switching between L/D inserts is as easy as removing the test section door and three screws holding the cavity insert to the model. A photo of the cavity installed in the test section is shown in Figure 2.3.

2.3 High Speed Pressure Transducers

Placed along the tube at various locations are piezoelectric pressure transducers. These pressure transducers provide both analog and digital data for each test run. The analog data allows for the observation of shock strength and the digital data allows for the calculation of shock velocity. When the shock passes by one of these sensors, it registers as a very sharp increase in pressure. Knowing the time at which these shocks arrive at the various transducer locations, along with the location of the transducers relative to each other allows for the shock speed calculation.

Ideally, calculating the time step between the arrival of each shock could be done by observing the time between the sharp spike in the analog pressure signal. However, to achieve a more accurate calculation of the time, a digital National Instruments data acquisition card with a maximum sampling frequency of 20 MHz was used. The faster sampling frequency allows the small time step to be calculated far more accurately than the analog National Instruments card used for the analog pressure signals.

In order to produce the digital signal required for the LabVIEW timer counter program to calculate the time between signals, a simple analog to digital circuit was designed. The design of the circuit was based on previous work done by Helen Huches [15]. This circuit, as shown in Figure 2.5, produces a 5V signal when an analog voltage is higher than a certain threshold. This threshold reference voltage is determined by three potentiometers connected to the circuit. The three potentiometers allow three different reference voltages to be set for up to six pressure transducer signals. When the analog voltage is lower than this reference voltage, the output of the circuit is 0V. This allows the digital data acquisition card to read either a HIGH (5V) signal or a LOW (0V) signal and interpret that as a digital signal.

This digital signal is also used to trigger the camera to record. The LabVIEW program, once getting a signal from a specified pressure transducer will generate a 5V TTL pulse.

2.3.1 Circuit

The circuit operates using three op-amps and one pull up resistor. The op-amps, as shown in the center of Figure 2.5, read the signal from the potentiometers. The voltage level, between 0 and 5 volts, from the potentiometer is set by the user. The op-amp compares this voltage to the voltage signal received through the BNC connectors. These BNC connectors are the analog voltage from the pressure transducers along the tube. If the voltage coming from the pressure transducers is below the voltage set by the user, the output of the circuit is 0V or a LOW digital signal. If the voltage is above this set voltage, the output of the circuit is 5V or a HIGH digital signal.

The potentiometers are put in place so the digital pulse is only sent when the shock wave passes by the transducer, rather than noise actuating the digital signal to be sent. Reliable results have been achieved with this circuit, but there are some cases in which this system has failed, but in Appendix A, it will be explained how to fix some of the more common problems and check for specific errors.

2.4 Infrared Sensor

Test time is important for the correlation of schlieren image data. Because the two systems are initiated simultaneously, the IR data corresponds easily to the image data. Knowing when the test gas reaches the model and for how long the test gas is flowing over the model allows for the extraction of frames that equate to just the test time. Although it is possible by inspection to see when the test gas arrives at the model, it

is not always obvious or as accurate. The arrival of the test gas produces shock waves at a different angle than the helium behind the incident shock wave, but this change in angle might not be very large, depending on the change in velocity. However, with the IR data, it can be closely estimated when the test gas should reach the model and for how long the model experiences the test gas.

Test time can be estimated using an X-T diagram. A sample X-T diagram is shown in Figure 3.6. This diagram is generated using compressible flow equations under an inviscid assumption. The lines represent important flow characteristics, including shock wave or expansion fan locations. The x-axis represents the spatial location along the tube, while the y-axis represents time. The time between the second and third line at the test section location represents the time which the test gas passes by the test section at the proper conditions. This ideal test time can be used to estimate the experimental test time, but a more accurate measurement of test time using the IR sensor is needed for proper image correlation and analysis.

The sensor used with the expansion tube at Lafayette is a Judson J10D series Indium Antemonide (InSb) sensor. These detectors have photovoltaic sensors that produce a current when exposed to infrared radiation. The sensor has the ability to be utilized for both absorption as well as emission sensing techniques. These techniques are explained in detail in a subsequent subsection.

2.4.1 Design of System

The alignment and placement of the various components is important for the proper collection of the IR light from the tube. The setup, as depicted in the diagram in Figure 2.7, includes a slit, a concave mirror, and a flat mirror. The slits affect the spacial

resolution of the incoming signal. If the slits are too wide, the sensor captures some of the scattered light, which shows up as a gradual increase in signal. If the slits are too narrow, not enough light can be captured by the sensor to show a good signal. The slit width is still being fine-tuned for the system in place, but the typical width for the slits is between 1 and 3 mm [18].

The sensor itself has a circular pickup area of about 2mm in diameter. Because of this, the IR light from the tube needs to be focused. Once the light passes through the slits, it reflects off of a concave mirror. This concave mirror, with a focal length of 200mm, focuses the light to a small point, just about the size of the sensor. The flat mirror is used to collapse the system so it can fit in a relatively small area. The entire system is contained in a box, as shown in Figure 2.8. Both mirrors are gold coated, as gold is very efficient at reflecting IR light. Since most of the testing is done during the day, a box was constructed to block out any ambient light from the room. The system is attached to the support structure of the tube by a 1/2" aluminum plate cantilever. Some bending, less than 1/16", is present at the end of the beam where the setup is supported, but it is not enough to affect the collection by the IR system.

2.4.2 Absorption

One method of data capturing that can be used is infrared absorption. The absorption method is based on the principle that different gases absorb radiation at different amounts. For absorption tests, an infrared light is placed behind a sapphire window on the side of the tube opposite the sensor. This IR light source provides the sensor with a baseline IR emission reading. As different gases pass by the sensor, they absorb some of the IR light, resulting in a different level of IR signal at the sensor. The time at which the absorption signal is level and highest corresponds to the test gas, and thus, the test

time within the test section. Although the sensor is capable of reading the IR signal with this method, the emission method has provided more reliable measurements of test time. The emission method only allows for signal to come to the sensor when the hot test gas is passing by, whereas the absorption method also shows when the other gases pass by the sensor. A typical voltage trace of the absorption method is shown in Figure 2.9. The change in voltage indicates that something had passed by the sensor, but the signal does not level off as expected. It can be seen that there is much uncertainty of which test gases are passing by the IR sensor during this pressure trace. There are no sharp spikes in signal, but rather, the signal exhibits low sloped voltage changes. Also, at the end of the test, the IR signal should return to its baseline (-4.2V for this test). However, the signal continues to rise, and even experiences a hump near the end of the test. This uncertainty in the voltage trace made it difficult to experimentally measure test times. Because of this, the emission method has been used primarily in the non-combusting tests and will continue to be used in the combustion tests. The emission signals captured are more reliable and provide a much clearer representation of the test gas flow in the tube. Further testing and tuning of the system would be required to capture more meaningful information with the absorption method.

2.4.3 Emission

As gases are heated, they emit IR radiation at different wavelengths. Using a filter, other wavelengths that are not these specific wavelengths, will not pass to the detector. For the non-reacting flows, a 5% CO₂ in nitrogen mixture emits IR within a 180nm bandwidth centered at 4.248 μ m. Placing the filter in front of the sensor allows the sensor to detect when, and for how long, the test gas, CO₂, passes by the sensor. Knowing how long the gas passes by the sensor allows for a direct measurement of test time in the test section.

Due to the sensor's close proximity to the test section, the test time extracted from the IR data is very close to the test time for the models in the test section. An example of the voltage trace produced by the sensor using the emission method is shown in Figure 2.10.

It is also noted that the voltage trace does not exhibit sharp spikes in signal. This is due to the size of the slit width, which was too large for this test. This slit width allowed forward-scattered light to be picked up by the sensor. It was assumed that the true start of the signal is halfway up the slope, at about 2.5V for Figure 2.10. However, it is important to continue fine-tuning the system and the slit width in order to eliminate this uncertainty.

2.4.4 Premature Ignition

The IR sensor will also be used to determine if pre-combustion occurred during a test. It is expected that if the reaction combusts upstream of the test section, it will result in a very large spike in IR signal. This will indicate that combustion did not originate at the cavity, but rather upstream of the cavity. Since the combustion tests are being used to test the flame-holding characteristics of the cavity, it is imperative that ignition originates at the cavity.

2.5 Schlieren Imaging

The schlieren effect operates on the principle that light refracts in air due to changes in density. This can be observed firsthand on a hot day. The rippling effect one can see above a road on a hot day is the light refracting due to the different densities of the air, caused by differences in local air temperature. Schlieren imaging takes advantage of this

principle by placing a knife edge at the focal point of the system. As light is refracted due to a change in density, this light gets blocked out by the knife edge, showing up as a dark spot in the captured image. Light that is not refracted continues through to the camera unblocked.

The images captured for the tests were done so using a high speed camera with a z-type schlieren system. A diagram of the schlieren system at Lafayette can be seen in Figure 2.11. The camera used for image capturing is a Phantom Miro m310 camera, capable of taking images up to 250,000 fps. However, as the recording frame rate increases, the resolution of each image decreases. For testing, a nominal frame rate of 77,028 Hz was used, as this provided a sufficient frame rate without sacrificing too much resolution. The resolution at which the images were taken in this study is 256x128. A sufficient frame rate in this context is one in which one test is captured within 500-1,000 frames. Also, to observe the frequencies within the cavity, the frame rate must be several times higher than the expected frequency of the acoustic waves. With L/D of 5, 7, and 9 having expected frequencies of 30 kHz, 21.4 kHz, and 16.7 kHz, respectively, a frame rate of 77 kHz would provide between 3 and 5 frames to observe the propagation of the waves.

All images in this study were capture at an exposure time of $1.3 \mu\text{s}$. Initial tests captured at an exposure time of around $12 \mu\text{s}$ showed images that were blurred. These blurred images were the result of spatial changes too quick for the camera to capture at that exposure time. Thus, a blur results over the space in which the shock or object traveled in that amount of time. Ben-Yakar estimated the exposure time needed to capture clear images would be on the order of 500 ns [1]. However, due to the limitations of this camera, an exposure time of $1.3 \mu\text{s}$ can be achieved at the set frame rate and resolution. The images captured have some blur, but shock waves and acoustic waves can still be

observed. The blur presents uncertainty when attempting to observe the acoustic waves' frequency in the cavity. Because of this uncertainty, other data systems will be necessary to measure these frequencies.

This type of imaging is important to see the various shock waves produced during testing. Since shock waves produce very sharp density gradients, a system that is capable of capturing these density gradients at high speeds is very useful. Typical test time of the non-reacting tests, the time in which the model experienced the test gas, was on the order of about 300 microseconds. With this camera, nearly 23 images were captured for the test time. With this many frames, it was possible to time correlate the images as well as extract dominant frequencies within the cavities.

Further information about the system, including more detail on how the system works and how to calibrate and align the system at Lafayette can be found in Ray Sanzi's honors thesis [19].



FIGURE 2.1: Annotated photograph of the expansion tube at Lafayette College.

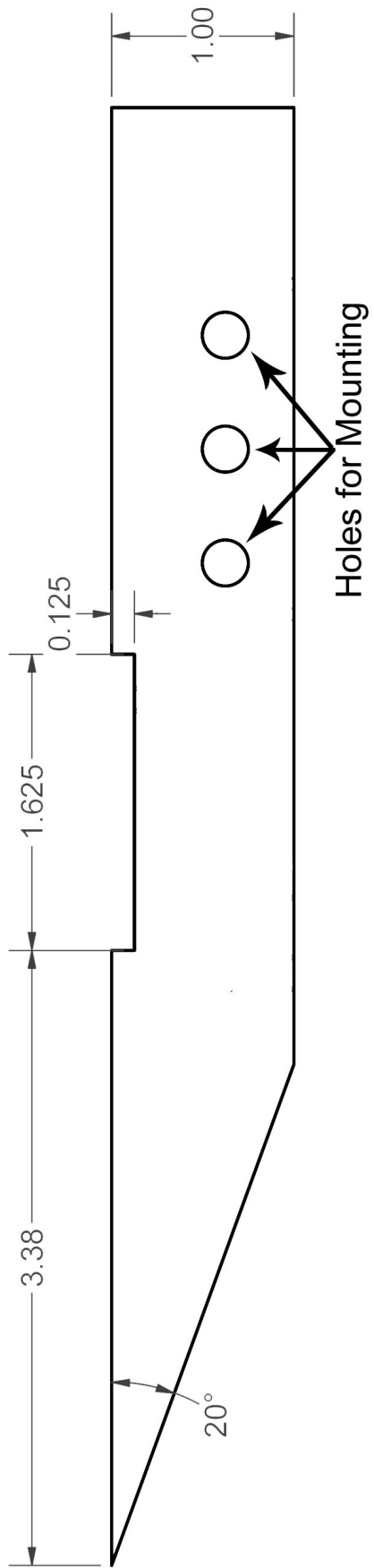


FIGURE 2.2: Dimensioned drawing of cavity used in testing. L/D = 13 with no insert.



FIGURE 2.3: Picture of cavity mounted in the test section.

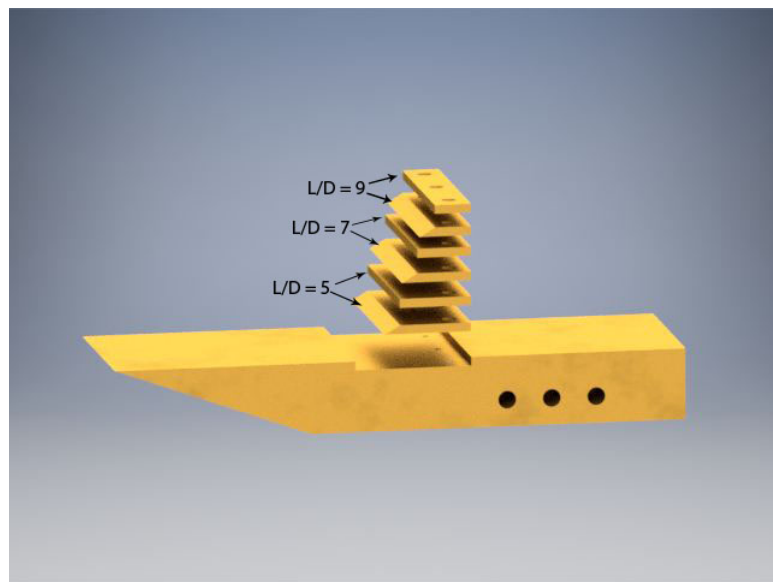


FIGURE 2.4: 3D rendering of cavity with various inserts to alter L/D.

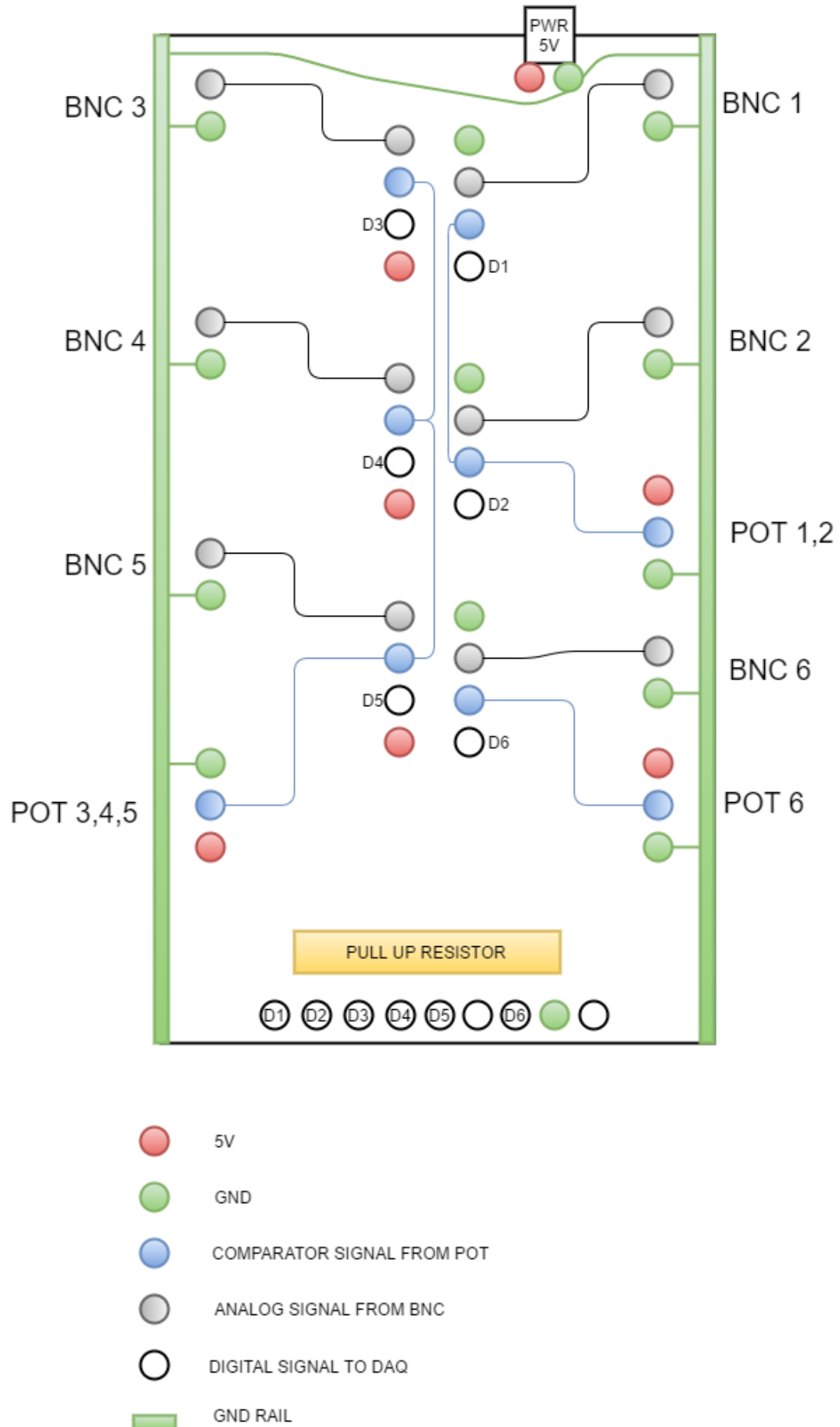


FIGURE 2.5: Circuit diagram for timer counter box.

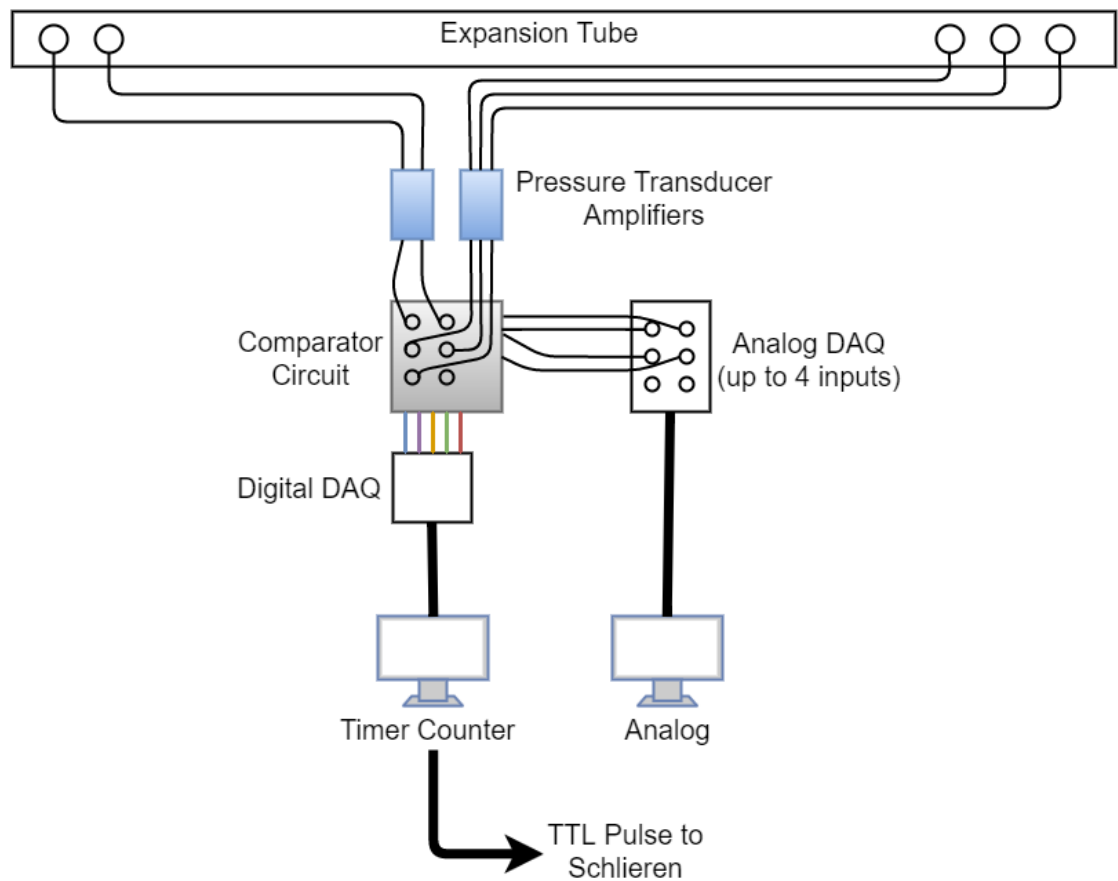


FIGURE 2.6: Data flow for high speed pressure transducers.

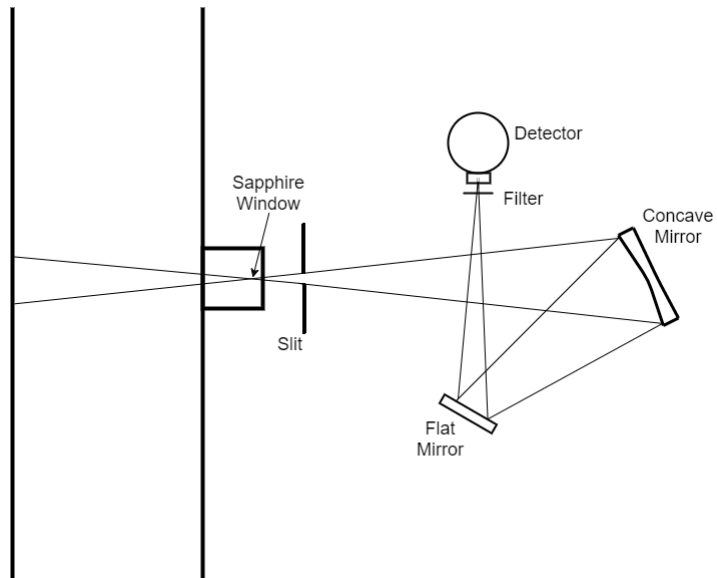


FIGURE 2.7: Schematic of the IR setup for the expansion tube.

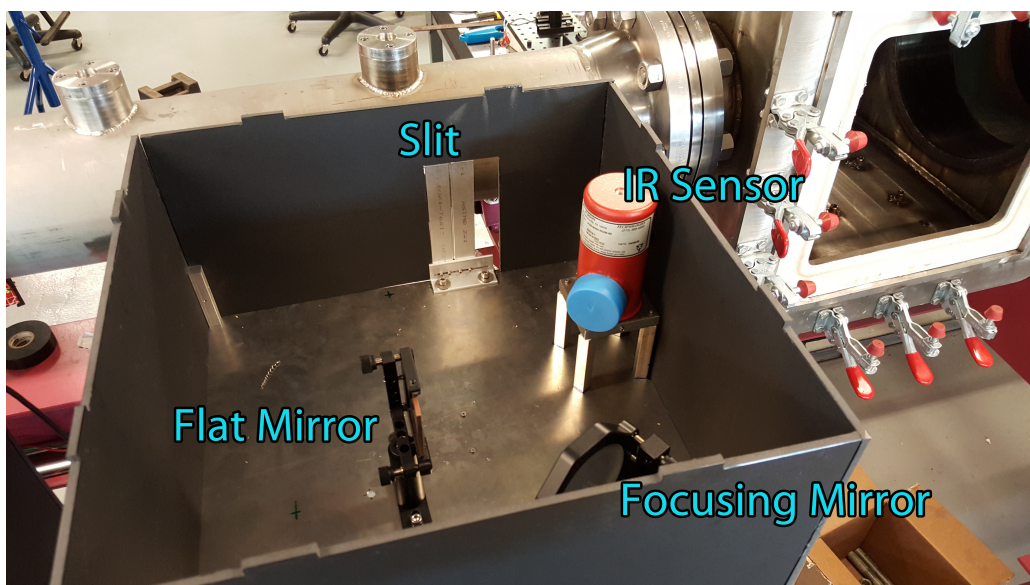


FIGURE 2.8: Photograph of actual IR setup in the lab.

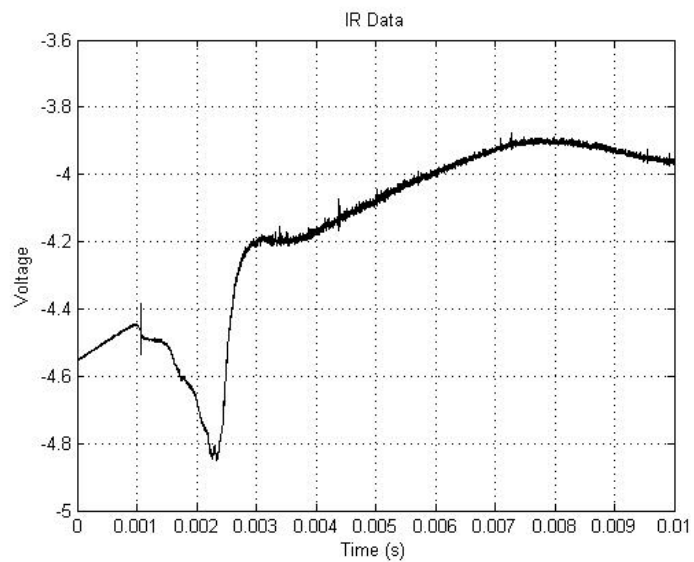


FIGURE 2.9: Typical IR data utilizing absorption method.

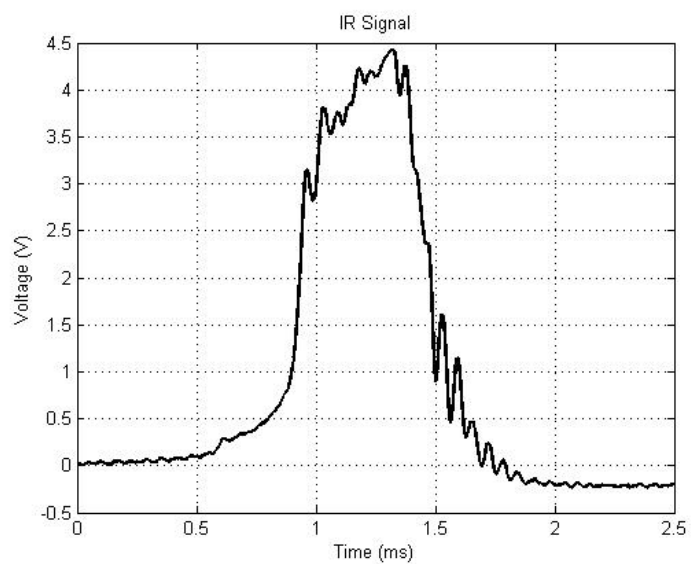


FIGURE 2.10: Typical IR data utilizing emission method.

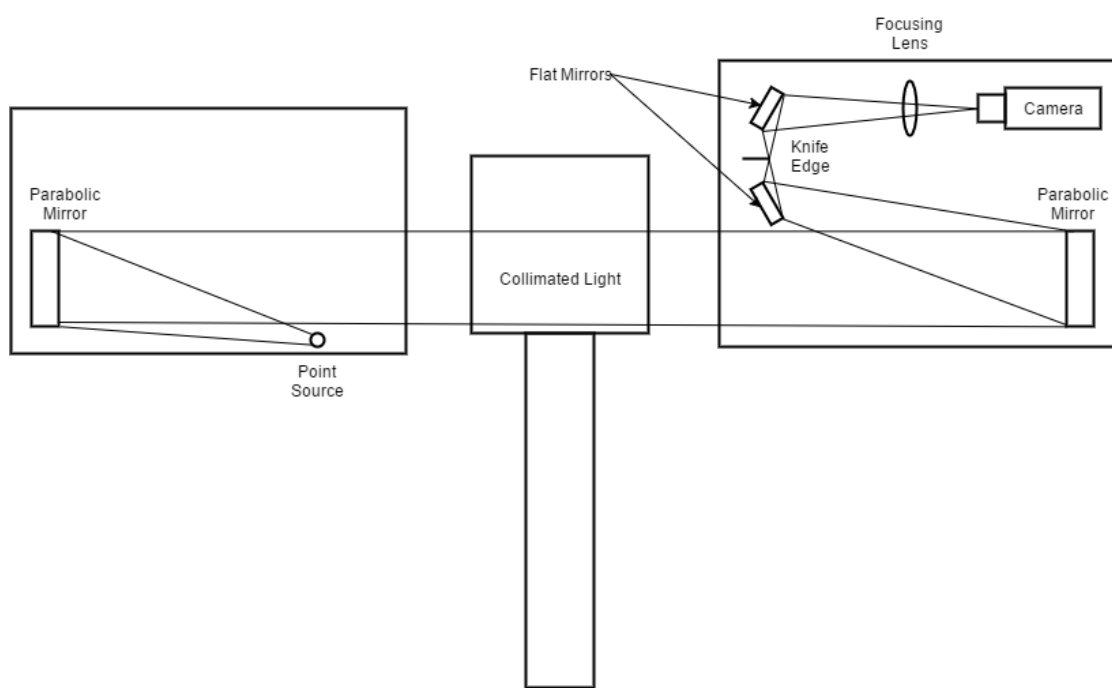


FIGURE 2.11: Diagram of schlieren system at Lafayette.

Chapter 3

Experimental Results

3.1 Non-Combusting Tests

In order to directly compare data between the different L/D ratios tested, it was important to keep the conditions nearly the same for all tests. For all non-combusting tests performed, the driver gas was helium at an initial pressure of 225 psi. The test gas was nitrogen at 0.5 psi and the expansion gas was helium at an initial pressure of 0.25 psi. This produced the freestream conditions as follows: $M_\infty = 2.32$, $U_\infty = 2150$ m/s, and T_∞ of 411K.

3.1.1 Schlieren

For each L/D, schlieren images were captured. Figures 3.1, 3.3, and 3.4 show the effects the L/D ratio has on mixing abilities. It can be observed that all of these cavities exhibit mixing and show signs of strong acoustic signals. The images captured for an L/D ratio of 5, however, show more disturbances, relatively, within the cavity itself. It is difficult

to say with the images, though, how much more mixing exists within the cavity. Further sharpening of the images

Figure 3.2 shows the cavity with an angled downstream wall. With this image, it is very clear that there are little or no acoustic waves present. This is strong evidence in support of the angled wall's ability to suppress the oscillation acoustic waves. However, with the acoustic waves not present, it may be possible that the mixing within the cavity suffers as a result. This will be investigated with the combustion tests in further studies.

Also captured by the schlieren imaging system is an indication of residence time within these cavities. Dust particles within the test section were dispersed in the flow and some of these particles were drawn into the cavity. Measuring how long these particles take to make one revolution within the cavity can provide an estimate of residence time. Figure 3.5 shows one such particle traveling over several images. The particle took 68 frames to make one revolution, corresponding to an estimated residence time of about $850 \mu\text{s}$. This corresponds well with the 1ms magnitude residence time achieved by Ben-Yakar [2].

3.1.2 IR

For some of these tests, IR emission data was captured to measure test time. The test times extracted from the IR data are displayed in Table 3.1. Of the test times which include nitrogen, they all correspond well to each other, which implies that conditions were reasonably the same for all tests. The theoretical test time, which was extracted from an X-T diagram, as shown in Figure 3.6, was about $559 \mu\text{s}$ for these tests. However, the compressible flow equations used in generating these X-T diagrams assume the flow to be inviscid. Due to viscous effects that are present in the tube along with non-ideal

TABLE 3.1: Test time from IR signal for various test gases. P4 = 225psi, P1 = 0.5 psi, $P_e = 0.25$ psi.

Test Number	Test Time (μs)	Test Gas
046	399	Nitrogen
048	443	Nitrogen
049	441	Nitrogen
050	424	Nitrogen
055	429	Nitrogen + CO ₂
056	434	Nitrogen + CO ₂
057	561	2H ₂ + O ₂ + 8N ₂
058	333	2H ₂ + O ₂ + 8N ₂ followed by Nitrogen + CO ₂

diaphragm breakage, the experimental test time achieved will be less than the theoretical test time, which is consistent with the data. It is important to note that even the tests without the CO₂ signal, the signal being picked up by the IR sensor was indicative of test time, as the test times extracted from these traces are consistent with the test times extracted from the traces with the CO₂ mixed with nitrogen. The signal captured from the nitrogen tests is presumed to be hot diaphragm particles flowing with the test gas from the upstream diaphragms.

Each test produced an IR trace similar to the one shown in Figure 3.7. As can be seen in this trace, the slit width was too wide for the test, so the IR sensor captured some light scattered forward, as indicated by the sloped increase in voltage signal. The test gas is indicated by the highest level of the signal. Test time is taken to be the time between points on the outside of the nearly flat level of signal. With this method, a consistent measure of test time can be achieved regardless of the amount of forward scattering of light. At this highest level, it is certain that there is only test gas passing by the sensor. With this method, the estimates of test time are conservative, but consistent. For further information on each IR test, please refer to the table in Appendix C.

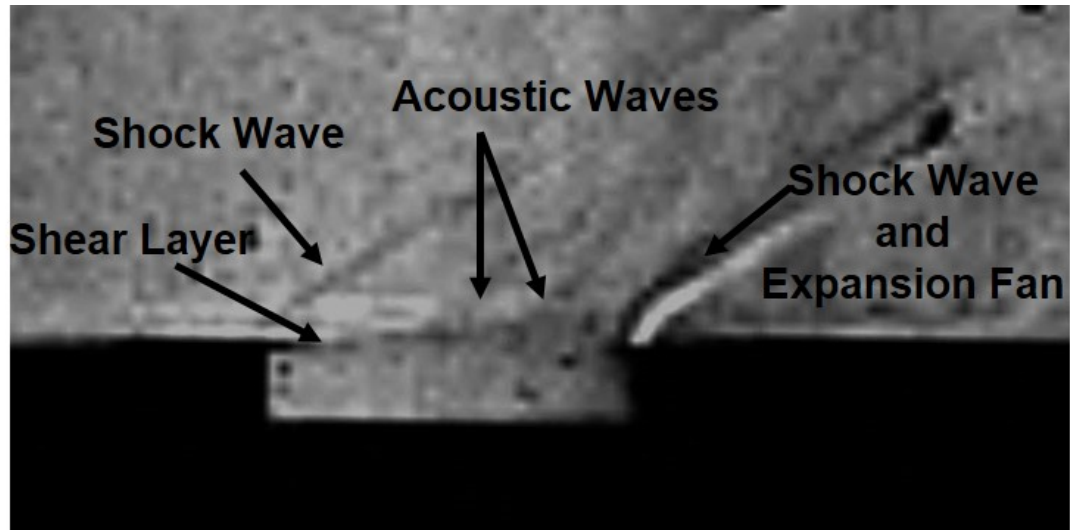


FIGURE 3.1: Schlieren image of cavity. $L/D = 5$.

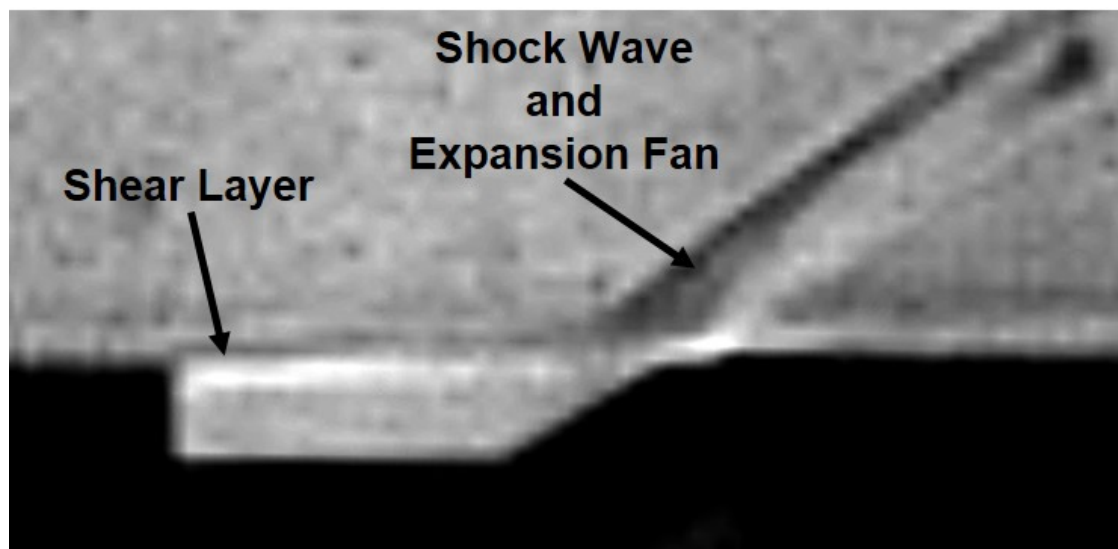


FIGURE 3.2: Schlieren image of cavity. $L/D = 5$. Downstream wall angle = 30°

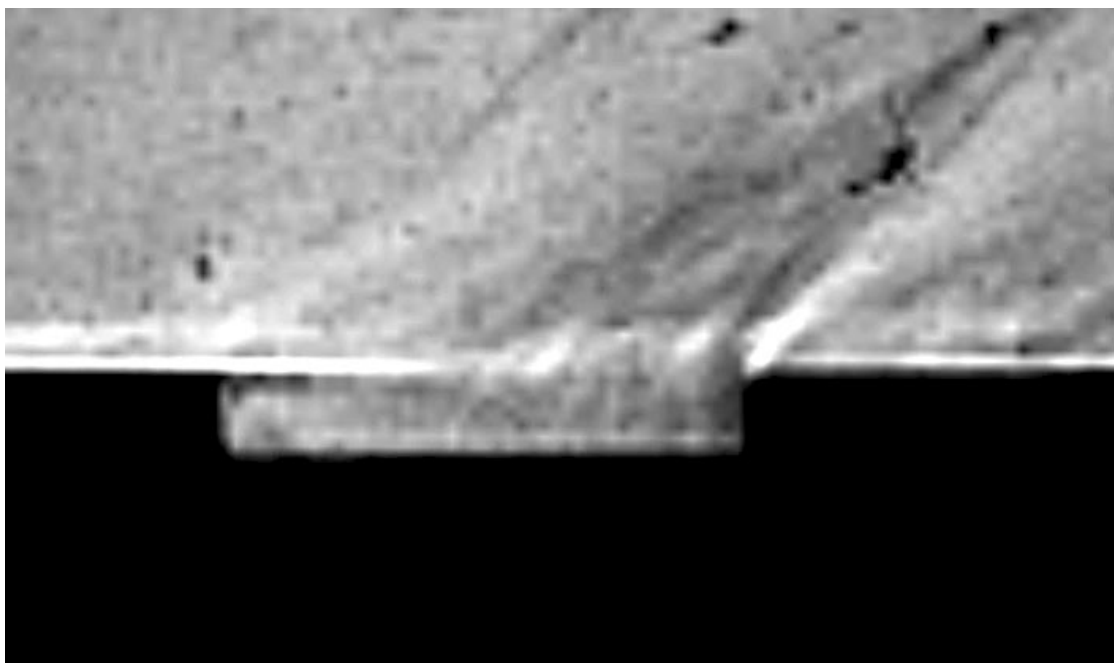


FIGURE 3.3: Schlieren image of cavity. $L/D = 7$.



FIGURE 3.4: Schlieren image of cavity. $L/D = 9$.

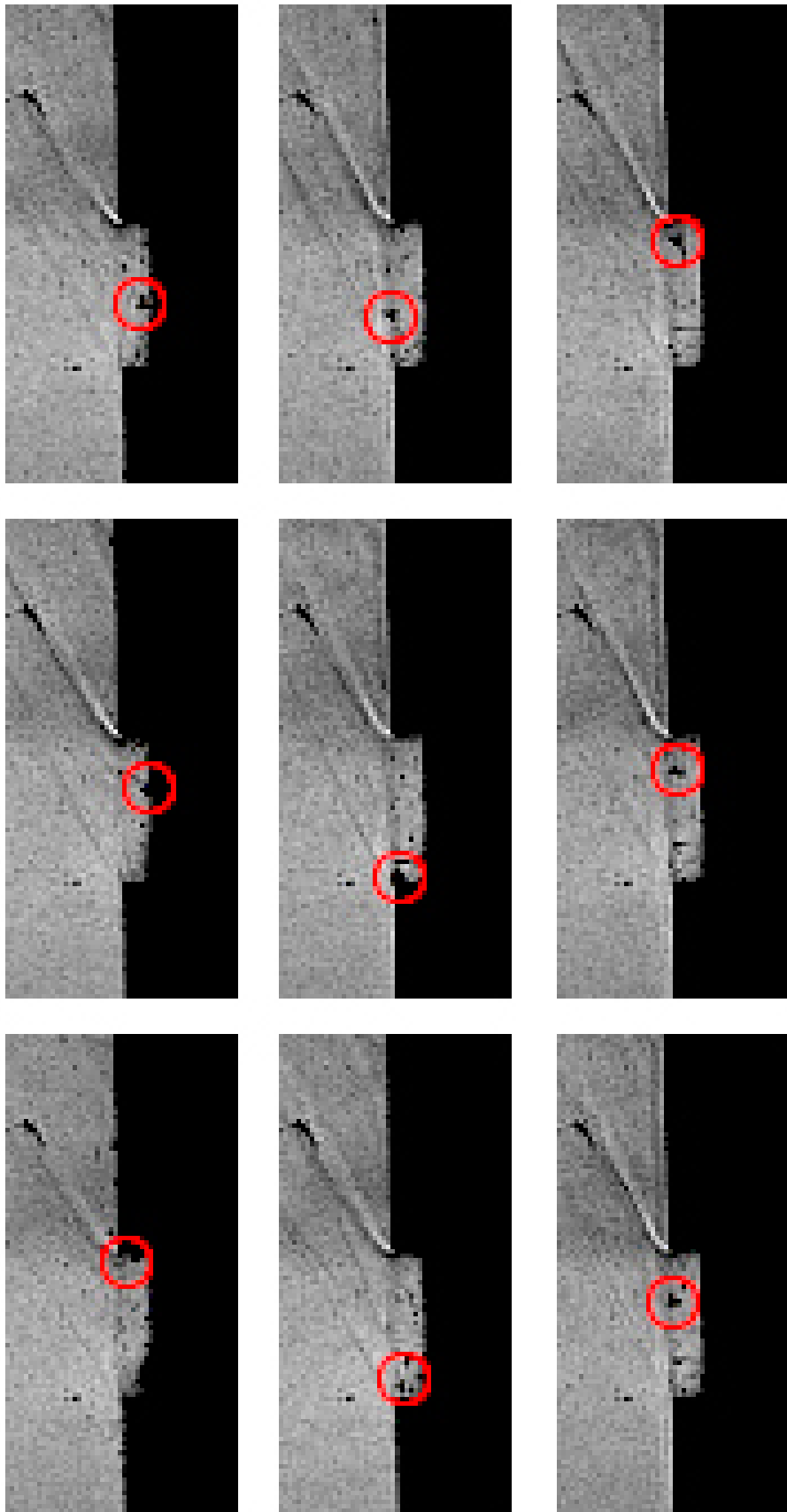


FIGURE 3.5: Time-correlated Schlieren image of cavity. $L/D = 5$. 9 frames out of 68 are shown. Residence time = $850 \mu\text{s}$.

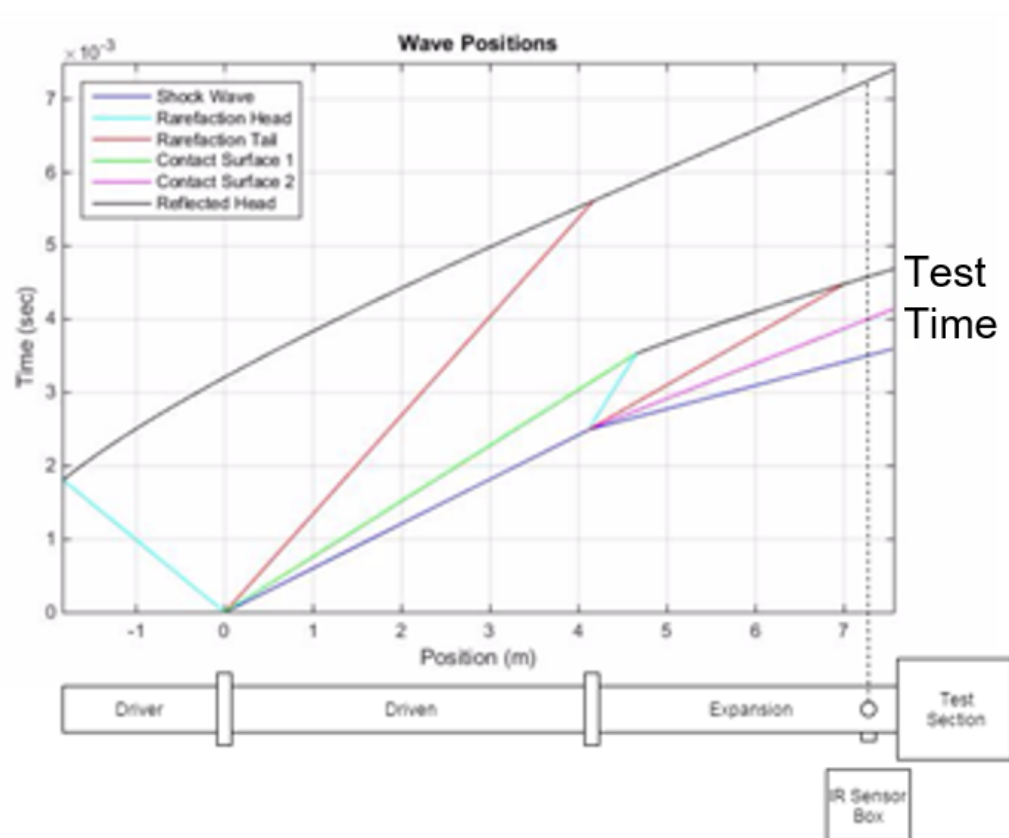


FIGURE 3.6: X-T diagram generated from the initial conditions of the cavity tests: $P_4 = 225\text{psi}$, $P_1 = 0.5\text{psi}$, $P_e = 0.25\text{psi}$. The test gas was nitrogen.

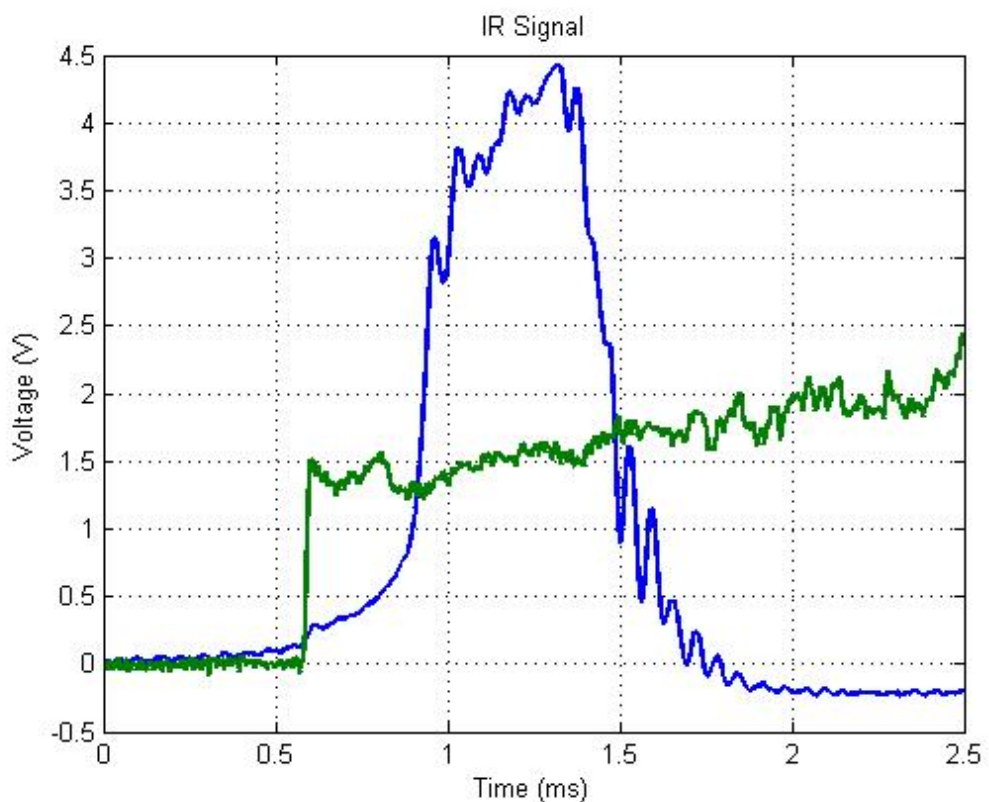


FIGURE 3.7: IR Signal for Test 056. $P_4 = 225\text{psi}$, $P_1 = 0.5\text{psi}$, $P_e = 0.25\text{psi}$. The test gas was a 95% nitrogen and 5% CO_2 mixture. Test Time = $434 \mu\text{s}$.

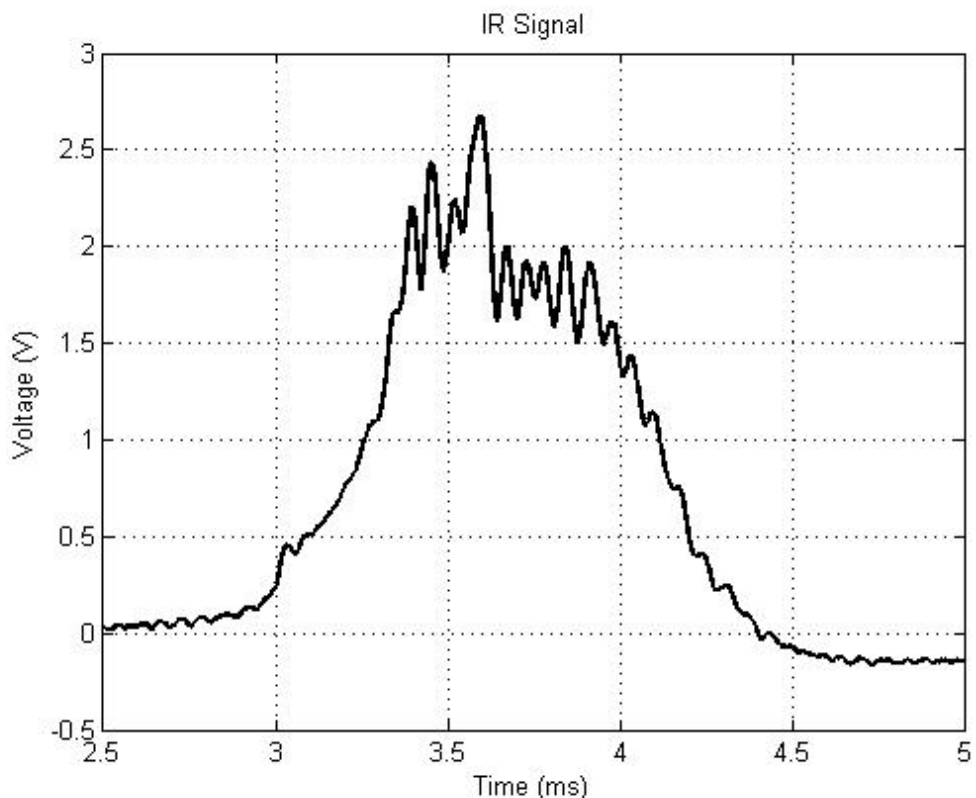


FIGURE 3.8: IR Signal for Test 057. $P_4 = 225\text{psi}$, $P_1 = 0.75\text{psi}$, $P_e = 0.25\text{psi}$. The test gas was a hydrogen and oxygen mixture followed by a 95% nitrogen and 5% CO_2 mixture. Test Time = $561 \mu\text{s}$.

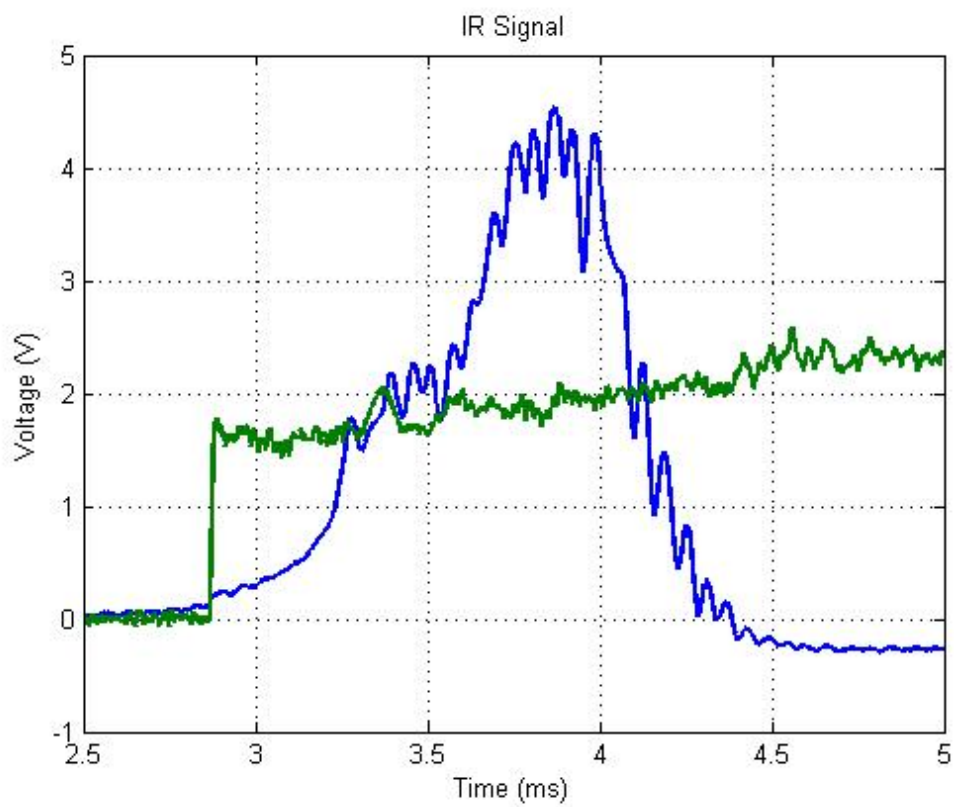


FIGURE 3.9: IR Signal for Test 058. $P_4 = 225\text{psi}$, $P_1 = 0.5\text{psi}$, $P_e = 0.25\text{psi}$. The test gas was a 95% Nitrogen and 5% CO_2 mixture. Test Time = $333 \mu\text{s}$.

Chapter 4

Future Work

4.1 Future Testing

Future tests would involve more of the combustion aspects of this investigation. Investigating the flame holding properties of these cavities will be important to understanding the interaction the acoustic waves with combustion. More tests need to be completed for the strong, stoichiometric mixture as the test gas. Each L/D should be tested, both with flat downstream walls as well as angled downstream walls.

Currently, there is work being performed within the LAUNCH team to introduce a PLIF imaging system, which will be able to utilize chemiluminescence to clearly image the combustion. Overlaying schlieren images with the PLIF images will give a clearer look at how the cavity is interacting with the flow, and how combustion is initiated and sustained.

4.2 Suggestions for Other Improvements

Further testing can be done beyond the weak combustion to further the understanding of this investigation. Much of the data from this study, as related to cavity frequencies, is entirely qualitative. The analysis of this study was done by comparing relative strengths of waves seen in Schlieren imaging. It would be good to have more quantitative data to validate the qualitative data captured by the high speed camera. To do this, a pressure transducer can be mounted within the cavity model.

Along with capturing quantitative data, testing true engine conditions would be the ultimate goal of these cavity tests. These engines do not have a well-mixed fuel and air mixture coming directly into the cavity itself. Incorporating jets of fuel into the system and having positive data showing enhanced mixing and combustion would show that these cavities could be used effectively in scramjet engines. Further details about both of these improvements are explained in the subsequent sections.

One way in which quantitative data could be used in conjunction with the qualitative data captured by the high speed camera would be to mount a pressure transducer within the cavity. A pressure transducer could have the potential to show the strengths of these pressure oscillations. Also, analyzing the pressure data could lead to accurate measurements of the frequency of the waves within the cavity.

Another approach to determining more accurately the frequency of the waves within the cavity could be by using a microphone in the test section. One research team used a microphone in the test section to capture the frequency of the acoustic waves produced by these cavities [20]. In their tests, they placed the microphone near the cavity to measure frequencies that it produced. Using a Fourier transform, they were able to locate which specific frequencies were dominant and the amplitudes of these

frequencies. A microphone within the test section might be a good option for non-invasive frequency measurements. The challenges associated with using a microphone in the test section are protecting the microphone from flying diaphragm particles as well as the high temperatures experienced in the test section.

4.2.1 Fuel Injection into Cavities

In order to fully understand the mixing effects of these cavities as they apply to real-world engines, it is important to understand that these engines inject the fuel into the freestream air. To investigate these cavities further, the test gas can be changed to an air mixture and the hydrogen fuel can be injected through the model upstream of the cavity. However, with the introduction of the jet-in-crossflow injections, there are other flow characteristics introduced, including bow shocks produced by the injected fuel. Currently, there is research being done by a member of the LAUNCH team on the jet-in-crossflow phenomenon. The combination of research could yield significant results that would directly applicable to the understanding of how these engines could be improved with respect to flame holding within the engine.

Appendix A

Implementation and Troubleshooting of the Timer Counter Circuit

When using the timer counter box, make sure the box is plugged into the power supply.

Once the box has power, turn on the power supply associated with the inverting circuit.

Once these are powered, the blue amplifier boxes should be turned on to supply power to the transducers. Set the appropriate gains on these boxes. The appropriate gains are based on what magnitude signal is desired. The LabVIEW program will only read signals between 0 and 5V. The pressure transducers output 0-5V for a pressure range of 0 to 100 psi. However, the pressure these transducers will be exposed to are only between 10 and 20 psi, resulting in a 0.5 to 1V signal. Setting the gain to 5 allows that signal to be amplified to between 2.5 and 5V. Having a larger signal allows for the comparator circuit to operate more easily. One can set the comparator nominal voltage with confidence, as the larger signal allows for a larger margin of error on the

set comparator voltage. This gives more confidence that the signal coming into the comparator circuit will be large enough to trigger a digital signal.

Once the physical systems are powered and ready, run the two LabVIEW programs for the capturing of the digital signals as well as the analog signals. The analog program filename is "BasicHighSpeedOscilloscope-fixed.vi" and the digital program filename is "CountersWorking.vi" For the analog signal, an input is required for sampling rate and time to take data. The typical sampling rate and time for tests is 1MHz and 10,000 μ s. The digital program asks for a user input of "milliseconds to wait." This is the amount of time the program should wait until sending the 5V TTL pulse to the camera. Typically, this value is set to 0.

One common problem with this circuit is that no digital signal is sent from the circuit itself. To check for this, use a function generator and an oscilloscope. Hook up the oscilloscope to one of the digital out wires of the box as well as the output of the function generator. Table A.1 shows the number of the digital out wire to its corresponding number. Attach the function generator to the corresponding BNC connector. A T-connector is needed to split the output signal from the function generator. Send a 5V amplitude sine wave from the function generator. The corresponding signal from the box should be a square wave. If there is no square wave present, check that the potentiometer is not too high or too low. The square wave should get wider or narrower depending on the position of the potentiometer. If there is still no signal coming from the box, there may be a burnt out op-amp. If, however, there is no signal coming from any of the outputs, it is unlikely all of the op-amps burned out. In this case, there may be a wiring issue. For this, check continuity between the signal coming in and the signal coming out to make sure voltages at each connection are what they are supposed to be.

TABLE A.1: Digital Out Pin Colors on the comparator circuit box corresponding to their Analog In numbers

Analog In	Digital Out
1	Blue
2	Purple
3	Black
4	Yellow
5	White
6	Red
GND	Green
Extra	Orange

Some alteration of the circuit may be required in this case. However, that is unlikely, and the problem is likely to be that the potentiometer level was set too high.

Appendix B

Implementation of the IR Sensor

To achieve the sensitivity required for the sensor, the operating temperature of the IR detector is about 77K, and the detector must be cooled with liquid nitrogen. Using the funnel to avoid spillage of the liquid nitrogen onto the cable connections or viewing window of the sensor, a few hundred milliliters were poured into the hole at the top of the sensor. When the sensor reaches the correct temperature, an eruption of cool gas occurs. It is important to wait until this eruption completes because the buildup of gas can cause the cap to blow off. Once the eruption subsides, the cap can be replaced to the top of the sensor and power can be supplied to the amplifier.

The amplifier can be utilized in two settings, AC or DC coupled. AC coupling, uses an extra capacitor to filter the DC component out of a signal containing both AC and DC elements. DC coupling allows for both the AC and DC elements to pass. The main consideration for the IR sensor, though is the gain present at each of the coupling settings. AC coupling introduces a 10x gain to the signal, which is useful, as the level of the emission signal is relatively low, at less than 0.5V. Although DC coupling could be utilized, the gain on the amplifier provides a stronger signal to analyze. For typical

IR emission tests, be sure the amplifier is set to AC coupled. If the IR sensor is to be run in absorption mode with the IR light source, DC coupling should be used, as the light source provides a relatively large base signal. To switch between AC and DC coupling, simply plug the cable that goes between the amplifier and the IR sensor into the appropriately labeled spot on the amplifier.

After power is supplied to the sensor through the amplifier, it is important to check that the system is aligned. Since the setup is attached to the support structure and not the tube itself, the recoil of the tube or the moving of the tube to replace diaphragms can alter the alignment of the window to the focusing mirror. To re-align the system, a stainless steel LED tube was constructed. This tube fits within the porthole on the back side of the tube, aligned with the port for the IR sensor. With the LED on and lined up with the inside wall of the far side of the tube, check the light source path. Be sure that the thin slit of red light hits the small sensor area. Adjust the flat mirror as needed to align the slit of red light with the IR sensor pickup area. Once the system is aligned, remove the LED tube and replace the plug in that port. The system at this point is aligned and ready for a test.

Appendix C

IR Test Information

TABLE C.1: Basic pressure, timer counter, IR, and test time data from all successful tests utilizing the IR sensor. The test gas labeled CO₂ was a 5% CO₂ mixture in nitrogen. The test gas labeled H₂ was a 2H₂ + O₂ + 8N₂ mixture. *Staged filling resulted in two levels of IR signal. The first number represents the time the Hydrogen mixture passed the sensor, while the second represents the CO₂ mixture.

Test No.	041	046	047	049	050	055	056	057	058
Test Gas	N ₂	CO ₂	CO ₂	H ₂	Staged				
P4 (psi)	225	225	225	225	226	225	224	225	223
P1 (psi)	0.5	0.51	0.5	0.5	0.75	0.51	0.5	0.75	0.76
Pe (psi)	0.5	0.25	0.25	0.25	0.25	0.26	0.26	0.28	0.25
T1 (s)	189	210	N/A	N/A	N/A	223.4	205.9	184.9	903.2
T2 (ms)	2.47	N/A	N/A	N/A	N/A	1.73	1.67	1.7733	1.67
T3 (s)	147	N/A	N/A	N/A	N/A	157.7	147.2	170.4	150.5
T4 (s)	148	153	N/A	N/A	N/A	160.1	150.9	171.3	150.0
IR Time (s)	467	399	466	436	424	429	434	561	333, 473*
Test Time (s)	363	551	544	544	659	544	538	676	N/A

Bibliography

- [1] Adela Ben-Yakar. *Experimental Investigation of Mixing and Ignition of Transverse Jets in Supersonic Crossflows*. PhD thesis, Stanford University, 2000.
- [2] Adela Ben-Yakar and Ronald K Hanson. Cavity flame-holders for ignition and flame stabilization in scramjets: an overview. *Journal of Propulsion and Power*, 17(4):869–877, 2001.
- [3] Hyungrok Do. *Plasma-Assisted Combustion in a Supersonic Flow*. PhD thesis, Stanford University, 2009.
- [4] Ibrahim Yilmaz, Ece Ayli, and Selin Aradag. Investigation of the effects of length to depth ratio on open supersonic cavities using cfd and proper orthogonal decomposition. *The Scientific World Journal*, 2013, 2013.
- [5] O Haldun Unalmis. Cavity oscillation mechanisms in high-speed flows. *AIAA Journal*, 42(10):2035–2041, 2004.
- [6] H Heller and J Delfs. Letter to the editor: Cavity pressure oscillations: the generating mechanism visualized. *Journal of Sound and Vibration*, 196(2):248–252, 1996.

- [7] David R Williams, Daniel Cornelius, and Clarence W Rowley. Supersonic cavity response to open-loop forcing. In *Active Flow Control*, pages 230–243. Springer, 2007.
- [8] O Wayne McGregor and RA White. Drag of rectangular cavities in supersonic and transonic flow including the effects of cavity resonance. *AIAA Journal*, 8(11):1959–1964, 1970.
- [9] ShiBin Luo, Wei Huang, Jun Liu, and ZhenGuo Wang. Drag force investigation of cavities with different geometric configurations in supersonic flow. *Science China Technological Sciences*, 54(5):1345–1350, 2011.
- [10] N Sato, A Imamura, S Shiba, S Takahashi, M Tsue, and M Kono. Advanced mixing control in supersonic airstream with a wall-mounted cavity. *Journal of Propulsion and Power*, 15(2):358–360, 1999.
- [11] JE Rossiter. Wind tunnel experiments on the flow over rectangular cavities at subsonic and transonic speeds. Technical report, Ministry of Aviation; Royal Aircraft Establishment; RAE Farnborough, 1964.
- [12] MR Gruber, RA Baurle, T Mathur, and K-Y Hsu. Fundamental studies of cavity-based flameholder concepts for supersonic combustors. *Journal of Propulsion and Power*, 17(1):146–153, 2001.
- [13] Stanford University. URL <https://web.stanford.edu/group/fpc/cgi-bin/fpcwiki/Main/Research>. [Online; accessed April 26, 2016].
- [14] Eli Lazar, Gregory Elliott, and Nick . Glumac. Control of the shear layer above a supersonic cavity using energy deposition. *AIAA journal*, 46(12):2987–2997, 2008.

- [15] Helen Hutchens. Theory, design, construction, and testing of an expansion tube. Master's thesis, Lafayette College, 2015.
- [16] RC Hibbeler. Mechanics of materials (2013).
- [17] Yunus A Cengel. *Fluid mechanics*. Tata McGraw-Hill Education, 2010.
- [18] William L Flower. *Experimental Study of Nitric Oxide Hydorgen Reaction Kinetics*. 1976.
- [19] Raymond Sanzi III. Working title. Master's thesis, Lafayette College, 2016.
- [20] KH Yu and KC Schadow. Cavity-actuated supersonic mixing and combustion control. *Combustion and Flame*, 99(2):295–301, 1994.